

# An amplitude equation modeling the single-to-double crest wave transition in orbital shaken cylindrical containers

Alessandro Bongarzone<sup>1</sup>, Margherita Guido<sup>2,3</sup> and François Gallaire<sup>1</sup>†

<sup>1</sup>Laboratory of Fluid Mechanics and Instabilities, École Polytechnique Fédérale de Lausanne, Lausanne, CH-1015, Switzerland

<sup>2</sup>Swiss Plasma Center, École Polytechnique Fédérale de Lausanne, Lausanne, CH-1015, Switzerland

<sup>3</sup>Numerical Algorithms and High-Performance Computing, École Polytechnique Fédérale de Lausanne, Lausanne, CH-1015, Switzerland

(Received xx; revised xx; accepted xx)

The container motion along a planar circular trajectory at a constant angular velocity, i.e. *orbital shaking*, is of interest in several industrial applications, e.g. for fermentation processes or in cultivation of stem cells, where good mixing and efficient gas exchange are the main targets. Under these external forcing conditions, the free surface typically exhibits a primary steady state motion through a single-crest dynamics, whose wave amplitude, as a function of the external forcing parameters, shows a Duffing-like behaviour. However, previous experiments in lab-scale cylindrical containers have unveiled that, owing to the excitation of super-harmonics, diverse dynamics are observable in certain driving-frequency ranges. Among these super-harmonics, the double-crest dynamics is particularly relevant, as it displays a notably large amplitude response, that is strongly favored by the spatial structure of the external forcing. In the inviscid limit and with regards to circular cylindrical containers, we formalize here a weakly nonlinear analysis via multiple timescale method of the full hydrodynamic sloshing system, leading to an amplitude equation suitable to describe such a super-harmonic dynamics and the resulting single-to-double crest wave transition. The weakly nonlinear prediction is shown to be in fairly good agreement with previous experiments described in the literature. Lastly, we discuss how an analogous amplitude equation can be derived by solving asymptotically for the first super-harmonic of the forced Helmholtz–Duffing equation with small nonlinearities.

**Key words:**

## 1. Introduction

Orbital shaking is a method to gently mix the liquid content of a container by its displacement at fixed container orientation along a circular trajectory and at a constant angular velocity. It is used in biological and chemical industrial applications, notably bacterial and cellular cultures (McDaniel & Bailey 1969; Wurm 2004), as an alternative

---

† Email address for correspondence: francois.gallaire@epfl.ch

to stirred tanks, where the liquid agitation results from a rotating impeller or the rotation of magnetic rod. In these cultivation protocols, cells are in suspension in the extracellular liquid medium, which serves as buffer for consumables from which they feed and for their secretions. The motion of the liquid prevents sedimentation and homogenizes the concentration of dissolved oxygen and nutrients and of secreted proteins and carbon dioxide. Thanks to the possible gas exchanges at the free surface, oxygen supply from the container bottom can possibly be circumvented, avoiding the formation of bubbles and thereby the damages that their collapse can exert on cells (Handa-Corrigan *et al.* 1989; Kretzmer & Schügerl 1991; Papoutsakis 1991), sparking interest in the development of large-scale, in the hectoliter range, orbital shaken bioreactors (Liu & Hong 2001; Jesus *et al.* 2004; Muller *et al.* 2007). It is therefore not a surprise if a significant body of research on the gas exchange and mixing in these devices has emerged over the last two decades (Büchs *et al.* 2000*a,b*; Büchs 2001; Maier *et al.* 2004; Muller *et al.* 2005; Micheletti *et al.* 2006; Zhang *et al.* 2009; Tissot *et al.* 2010; Tan *et al.* 2011; Tissot *et al.* 2011; Klöckner & Büchs 2012).

At a more fundamental level, the hydrodynamics of these orbital shaking devices has received recent attention, from both experimental (Reclari *et al.* 2014; Bouvard *et al.* 2017; Moisy *et al.* 2018) and theoretical (Reclari *et al.* 2014; Horstmann *et al.* 2020) perspectives, predominantly using linear potential flow models. These models are often complemented with effective viscous damping rates to incorporate the energy dissipation responsible for the phase-shifts between wave and shaker, which was also seen to be sometimes responsible for damping-induced symmetry-breaking linear mechanisms resulting in linear spiral wave patterns (Horstmann *et al.* 2020, 2021). Previous studies make mostly use of classical existing theories for general linear sloshing dynamics, reviewed for instance in Ibrahim (2005) or Faltinsen & Timokha (2009).

In order to refine the linear potential model and, specifically, to predict the occurrence of the super-harmonic wave dynamics observed experimentally, Reclari (2013) and Reclari *et al.* (2014) proposed an inviscid weakly nonlinear analysis based on a second order straightforward asymptotic expansion procedure, which was shown to be capable of capturing the observed resonance frequencies and of characterizing different multiple-crest wave patterns. Among these patterns, the super-harmonic double-crest wave dynamics is particularly relevant, as it appears to be the most stable and the one which displays the largest amplitude response. However, their analysis, as typical of straightforward asymptotic expansions, suffers from secular terms (Castaing 2005; Nayfeh 2008) and, therefore, it still fails in describing the correct nonlinear behaviour close to both harmonic and super-harmonic resonances.

This limitation was partially overcome by Timokha & Raynovskyy (2017) and Raynovskyy & Timokha (2018), who have applied the Narimanov–Moiseev multimodal sloshing theory (Narimanov 1957; Moiseev 1958; Dodge *et al.* 1965; Faltinsen 1974; Narimanov *et al.* 1977; Lukovsky 1990) describing the nonlinear wave dynamics near the first harmonic resonance, which was proven to be of the *hard*-spring type, in qualitative agreement with the observations of Reclari (2013) and Reclari *et al.* (2014). Nevertheless, they were not able to quantitatively compare their predictions with the latter experimental measurements because these were done for  $H = h/R \leq 1.2$ , e.g.  $H = 1$  and  $1.04$  (with  $h$  the fluid depth and  $R$  the container radius), where, as stated by the authors themselves, the adopted nonlinear modal equations are not applicable due to the secondary resonance phenomena (Faltinsen *et al.* 2016).

In the spirit of the aforementioned multimodal theory but with regards to square-base basins, the resonant amplification of higher order modes was investigated by Faltinsen *et al.* (2005), who formalized a so-called adaptive asymptotic modal approach capable to

improve the agreements with earlier experiments. Yet, to the knowledge of the authors, the adaptive modal approach was never extended to orbital shaken circular cylindrical containers.

For these reasons, it appears that a quantitatively accurate model for the prediction of the diverse wave dynamics observed during the thorough experimental campaign carried out by Reclari (2013) and Reclari *et al.* (2014) has not been provided yet.

The present work is precisely dedicated to the development of a weakly nonlinear analysis based on the multiple timescale method, which will be seen to successfully capture nonlinear effects for the main additive harmonic resonances as well as the more subtle additive and multiplicative resonance governing the super-harmonic double-crest saturation. Amplitude equations are rigorously derived in an inviscid framework, which once amended with an *ad-hoc* damping term as only tuning parameter, well match the experimental findings of Reclari (2013) and Reclari *et al.* (2014). Lastly, the obtained amplitude equations for harmonic single-crest and super-harmonic double-crest waves are found to be compatible with the two well known one-degree-of-freedom (1dof) systems, the Duffing and the Helmholtz-Duffing oscillators, respectively.

The manuscript is organized as follows. The flow configuration and governing equations are introduced in §2. §3 is dedicated to briefly summarize the salient points of the asymptotic model proposed by Reclari *et al.* (2014), whose limitations motivated the present work. After tackling the more common case of harmonic single-crest wave in §4.1, the weakly nonlinear amplitude equation governing the super-harmonic double-crest wave dynamics is derived in §4.2. Final comments and conclusions are outlined in §5.

## 2. Flow configuration and governing equations: potential model

We consider a cylindrical container of diameter  $D = 2R$  filled to a depth  $h$  with a liquid of density  $\rho$ . The air-liquid surface tension is denoted by  $\gamma$ . The orbital (circular) shaking motion (see sketch in figure 1) can be represented as the combination of two sinusoidal translations with a  $\pi/2$  phase shift, thus leading to the following equations of motion for the container axis intersection with the  $z = 0$  plane, parametrized in cylindrical coordinates  $(r, \theta)$

$$\dot{\mathbf{X}}_0 = \begin{cases} -\frac{d_s}{2} \Omega_d \sin(\Omega_d t - \theta) \mathbf{e}_r \\ \frac{d_s}{2} \Omega_d \cos(\Omega_d t - \theta) \mathbf{e}_\theta \end{cases}. \quad (2.1)$$

In the classical potential flow limit, i.e. the flow is assumed to be inviscid, irrotational and incompressible, the motion is described in terms of free surface deformation,  $\eta$ , and a potential velocity field,  $\Phi_{tot}$ , which is typically separated into a container,  $\Phi_c$ , and a fluid component,  $\Phi$ . Hence, the liquid motion within the moving container is governed by the Laplace equation,

$$\Delta\Phi = \frac{1}{r} \frac{\partial\Phi}{\partial r} + \frac{\partial^2\Phi}{\partial r^2} + \frac{1}{r^2} \frac{\partial^2\Phi}{\partial\theta^2} + \frac{\partial^2\Phi}{\partial z^2} = 0, \quad (2.2)$$

subjected to the homogeneous no-penetration condition,  $\nabla\Phi \cdot \mathbf{n} = \mathbf{0}$ , at the solid sidewall and bottom, and by the dynamic and kinematic free surface boundary conditions at  $z = \eta$  (see Ibrahim (2005)),

$$\frac{\partial\Phi}{\partial t} + \frac{1}{2} \nabla\Phi \cdot \nabla\Phi + \eta - \frac{\kappa(\eta)}{Bo} = r f \cos(\Omega t - \theta), \quad (2.3a)$$

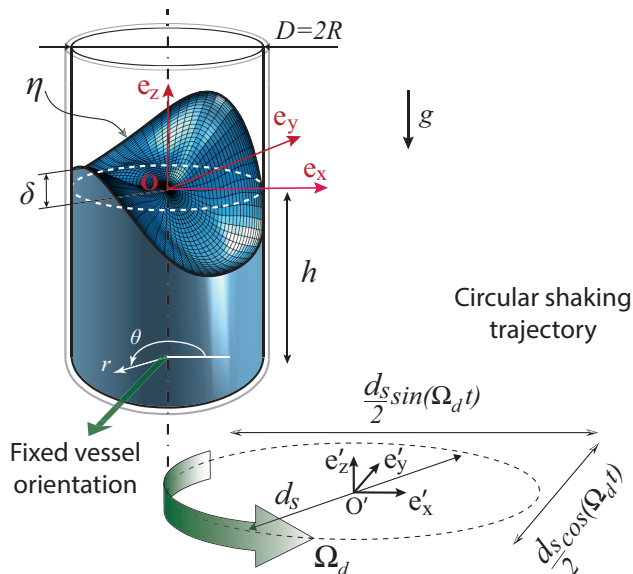


FIGURE 1. Sketch of a cylindrical container of diameter  $D = 2R$  and filled to a depth  $h$ . The gravity acceleration is denoted by  $g$ .  $O'e'_x e'_y e'_z$  is the Cartesian inertial reference frame, while  $Oe_x e_y e_z$  is the Cartesian reference frame moving with the container. The origin of the moving cylindrical reference frame  $(r, \theta, z)$  is placed at the container revolution axis and, specifically, at the unperturbed liquid height,  $z = 0$ . The perturbed free surface and contact line elevation are denoted by  $\eta$  and  $\delta$ , respectively.  $d_s$  is the diameter of the circular shaking trajectory, characterized by a driving angular frequency  $\Omega_d$ .

$$\frac{\partial \eta}{\partial t} + \frac{\partial \Phi}{\partial r} \frac{\partial \eta}{\partial r} + \frac{1}{r^2} \frac{\partial \Phi}{\partial \theta} \frac{\partial \eta}{\partial \theta} - \frac{\partial \Phi}{\partial z} = 0, \quad (2.3b)$$

which have been made non-dimensional by using the container's characteristic length  $R$ , the characteristic velocity  $\sqrt{gR}$  and the time scale  $\sqrt{R/g}$ . In (2.3a),  $\kappa(\eta)$  denotes the fully nonlinear curvature, while  $Bo = \rho g R^2 / \gamma$  is the Bond number. The non-dimensional driving amplitude and angular frequency read  $f = d_s \Omega_d^2 / (2g)$  and,  $\Omega = \Omega_d / \sqrt{g/R}$ , respectively. When surface tension is accounted for, an additional contact line boundary condition is required at  $z = \eta$  and  $r = 1$ , typically written as  $\partial \eta / \partial r = \cot \vartheta$ , where  $\vartheta$  is the macroscopic contact angle. Under the classic free-end edge contact line assumption with  $\vartheta = \pi/2$  adopted here, the latter dynamic equation simply reduces to  $\partial \eta / \partial r = 0$ . This means that the free surface at rest is flat and that a  $\pi/2$  static contact angle is maintained when the contact line elevation changes dynamically.

### 3. Linear solution and second-order straightforward asymptotic expansion

In order to enlighten the limitations of the expansion procedure developed by Reclari *et al.* (2014), which motivates the formalization of the new theoretical framework proposed in the present paper, we briefly recall the salient points. Let us consider the following asymptotic expansion for the flow quantities,

$$\Phi = \Phi_0 + \epsilon \Phi_1 + \epsilon^2 \Phi_2 + O(\epsilon^3), \quad (3.1a)$$

$$\eta = \eta_0 + \epsilon \eta_1 + \epsilon^2 \eta_2 + \mathcal{O}(\epsilon^3), \quad (3.1b)$$

together with the further assumption of small driving forcing amplitudes of order  $\mathcal{O}(\epsilon)$ , i.e.  $f = \epsilon F$ , with  $\epsilon$  a small parameter  $\epsilon \ll 1$ . Solution  $\mathbf{q}_0 = (\Phi_0, \eta_0)$  represents the rest state, which has a potential velocity field null everywhere,  $\Phi_0 = 0$ , and a flat interface,  $\eta_0 = 0$ , as the contact angle is here assumed to be  $\vartheta = \pi/2$ . Substituting the expansions above in equations (2.2)-(2.3b), a series of system at the various order in  $\epsilon$  is obtained. At leading order, equations (2.2)-(2.3b) reduce to a forced linear system, whose matrix compact form reads,

$$(\partial_t \mathcal{B} - \mathcal{A}) \mathbf{q}_1 = \mathcal{F}_1, \quad (3.2)$$

with  $\mathbf{q}_1 = \{\Phi_1, \eta_1\}^T$ ,  $\mathcal{F}_1 = F \{0, r/2\}^T e^{i(\Omega t - \theta)} + c.c. = F \hat{\mathcal{F}}_1^F e^{i(\Omega t - \theta)} + c.c.$  and

$$\mathcal{B} = \begin{pmatrix} 0 & 0 \\ I_\eta & 0 \end{pmatrix}, \mathcal{A} = \begin{pmatrix} \Delta & 0 \\ 0 & -I_\eta + \frac{1}{Bo} \frac{\partial \kappa(\eta)}{\partial \eta} \end{pmatrix}, \quad (3.3)$$

where *c.c.* stands for complex conjugate,  $\partial \kappa(\eta) / \partial \eta$  represents the first order variation of the curvature associated with the small perturbation  $\epsilon \eta_1$  and  $I_\eta$  is the identity matrix associated with the interface  $\eta$ . Note that the kinematic condition does not explicitly appear in (3.3), but it is enforced as a boundary condition at the interface (Viola *et al.* 2018). In the limit of zero external forcing, i.e.  $F = 0$ , system (3.2) is a linear homogeneous problem which, by seeking for solutions having the following normal form

$$\hat{\mathbf{q}}^{mn}(r, z) e^{i(\omega_{mn} t - m\theta)} + c.c., \quad (3.4)$$

reduces to the classic generalized eigenvalue problem for inviscid capillary-gravity waves

$$(i\omega_{mn} \mathcal{B} - \mathcal{A}_m) \hat{\mathbf{q}}^{mn} = \mathbf{0}, \quad (3.5)$$

where indices  $(m, n)$  represent the number of nodal circles and nodal diameters, respectively, with  $m$  also commonly known as azimuthal wavenumber. Owing to the normal mode expansion, we notice that the operator  $\mathcal{A}_m$  is complex, since  $\theta$  derivatives produce  $-im$  terms. An exact analytical solution to equation (3.5) can be readily obtained via a Bessel-Fourier-series representation leading to the well-known dispersion relation (Lamb 1993)

$$\omega_{mn}^2 = (k_{mn} + k_{mn}^3 / Bo) \tanh(k_{mn} H), \quad (3.6)$$

with  $H = h/R$  and where the wavenumbers  $k_{mn}$  is given by the  $n$ th-root of the first derivative of the  $m$ th-order Bessel function of the first kind satisfying  $J'_m(k_{mn}) = 0$ .

Despite the existence of this analytical solution, in this work we opt for a numerical scheme based on a discretization technique, where linear operators  $\mathcal{B}$  and  $\mathcal{A}_m$  are discretized in space by means of a Chebyshev pseudospectral collocation method with a two-dimensional mapping implemented in Matlab, which is analogous to that described by Viola *et al.* (2018). This numerical technique will enable us to avoid straightforward, but cumbersome calculations, otherwise required in the development of the rest of this work and, particularly, of section §4.2. One must note that when (3.5) is solved numerically as in the present case, additional boundary conditions need to be made explicit in order to regularize the problem on the revolution axis ( $r = 0$ ), i.e.

$$m = 0 : \quad \frac{\partial \hat{\eta}^{mn}}{\partial r} = \frac{\partial \hat{\Phi}^{mn}}{\partial r} = 0, \quad (3.7a)$$

$$|m| \geq 1 : \quad \hat{\eta}^{mn} = \hat{\Phi}^{mn} = 0. \quad (3.7b)$$

It is also useful to note that owing to the symmetries of the problem, system (3.5) is invariant under the transformation

$$(\hat{\mathbf{q}}^{mn}, +m, i\omega_{mn}) \longrightarrow (\hat{\mathbf{q}}^{mn}, -m, i\omega_{mn}). \quad (3.8)$$

Convergence of the numerical solution was checked by computing the first 16 modes ( $m = 0, 2, 3, 4$  with  $n = 1, 2, 3, 4$ ), whose corresponding natural frequency values,  $\omega_{mn}$ , matched the analytical ones given by (3.6) up to the fourth digit for a computational grid  $N_r = N_z = 60$ , with  $N_r$  and  $N_z$  the number of radial and axial grid points, respectively.

Let us now reintroduce the forcing term on the r.h.s. of equation (3.2). In contradistinction with the cases of unidirectional forcing (Miles 1984*a, b*), for circular orbits, given the azimuthal periodicity of the associated forcing, the shaking at linear order is expected to excite non-axisymmetric modes only and, specifically, those with  $m = 1$ . Therefore, the linear response to the external forcing can be sought as

$$\mathbf{q}_1 = F \hat{\mathbf{q}}_1^F e^{i(\Omega t - \theta)} + c.c., \quad (3.9)$$

with  $\hat{\mathbf{q}}_1^F$  being the solution of the following forced problem

$$(i\Omega\mathcal{B} - \mathcal{A}_1) \hat{\mathbf{q}}_1^F = \hat{\mathcal{F}}_1^F. \quad (3.10)$$

The response structure  $\hat{\mathbf{q}}_1^F$  is here computed numerically, but, in practice, it is formally equivalent to that obtained analytically by Reclari *et al.* (2014) by projecting the forcing term  $\hat{\mathcal{F}}_1^F$  onto the basis formed by the first order Bessel functions of the first kind, except that surface tension is retained here because of the finite Bond number. Noting that  $\epsilon F = f = d_s \Omega^2 / (2g)$ , in figure 2 the linear solution  $\epsilon \mathbf{q}_1^F$  from (3.9) is shown (black solid lines) and compared with experimental measurements reported by Reclari *et al.* (2014) in terms of maximum non-dimensional crest-to-trough contact line amplitudes,  $\tilde{\delta} = \delta R / D$ , with  $\delta(\theta, t) = \eta(r = 1, \theta, t)$ . Measurements for different values of the non-dimensional shaking diameters,  $\tilde{d}_s = d_s / D$ , are shown. Blue and green markers in figure 2 correspond to highly nonlinear scenarios manifesting a free surface breaking, which will be therefore ignored thereafter. As discussed by Reclari *et al.* (2014) and reproduced here, the linear solution describes well the single-crest (SC) wave dynamics for driving frequencies far enough from harmonic resonances and, particularly, for small  $\tilde{d}_s$ . However, as typical of undamped forced oscillators, the amplitude of the inviscid linear response to the external forcing is proportional to  $\propto 1 / (\omega_{1n}^2 - \Omega^2)$  and therefore it naturally diverges close to  $\omega_{1n}$ , thus failing in predicting the close-to-resonance behaviour, e.g. for  $\tilde{d}_s = 0.02$  at  $\Omega \approx \omega_{11}$ . Introduction of viscous dissipation would regularize the divergent behaviour at  $\Omega = \omega_{11}$ , however, in absence of any nonlinear restoring term, the *hardening* nonlinearity displayed in figure 2 cannot be retrieved.

Furthermore, in experiments multiple-crested waves were observed at fractions of the natural frequencies (red markers in figure 2), i.e. the system responds with a frequency which is  $n$ -times (with  $n$  positive integer) that of the external forcing. Here we refer to such conditions as super-harmonic dynamics (note that the terminology sub-harmonic was used by Reclari *et al.* (2014) instead). Among these super-harmonics, the double-crest (DC) wave dynamics, occurring at a driving frequency  $\Omega \approx \omega_{21} / 2$ , was seen to be the most relevant (see figure 2), i.e. the most stable and the one displaying the largest deviation from the linear approximation. This specific multiple-crest dynamics, which is intrinsically nonlinear, is indeed favored by the azimuthal symmetry of the external forcing. Reclari *et al.* (2014) tentatively described such a double-crest dynamics

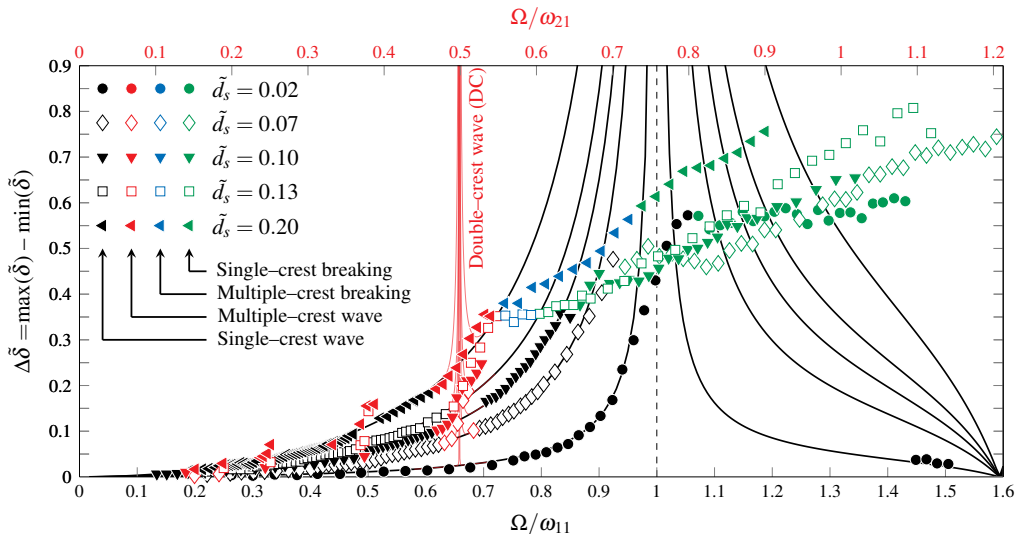


FIGURE 2. Markers correspond to the experimentally measured maximum crest-to-trough contact line amplitude (non-dimensional), with  $\bar{\delta} = \delta R/D = \delta/2$ , reported by Reclari *et al.* (2014) for two container diameters,  $D = 0.144$  m and  $D = 0.287$  m, a non-dimensional depth  $\bar{H} = h/D = 0.52$  and five values of  $\bar{d}_s = d_s/D$ , as a function of the non-dimensional shaking frequency  $\Omega$  normalized by the natural frequency of the first non-axisymmetric mode,  $\omega_{11} = 1.3286$  ( $m = 1$ ) on the bottom-x-axis and by that of first non-axisymmetric mode with  $m = 2$ ,  $\omega_{21} = 1.7475$ , on the top-x-axis (the frequency values correspond to  $D = 0.287$  m). Colors denote different wave conditions. Black solid lines: linear potential model solution, from (3.9), computed by solving numerically equation (3.10). Red solid lines: weakly nonlinear solution close to the  $\Omega \approx \omega_{21}/2$ , obtained by computing (3.14). Note that in order to ease the comparison with experiments, the non-dimensional  $\delta$  was rescaled by a factor  $R/D = 1/2$ , as the container diameter  $D$ , rather than the container radius  $R$ , was used by Reclari *et al.* (2014) to make the equations non-dimensional.

by pursuing the asymptotic analysis up to the second order in  $\epsilon$ , as in equations (3.1a) and (3.1b), in order to account for second order system weak nonlinearities.

At the second order in  $\epsilon$ , one obtains the following forced linear system,

$$(\partial_t \mathcal{B} - \mathcal{A}) \mathbf{q}_2 = \mathcal{F}_2 = F^2 \left( \hat{\mathcal{F}}_2^{FF} e^{i(2\Omega t - 2\theta)} + c.c. \right) + F^2 \hat{\mathcal{F}}_2^{F\bar{F}}, \quad (3.11)$$

where  $\mathcal{F}_2$  gathers a series of terms produced by the first order solution through the second order system nonlinearities. For the sake of brevity, the explicit expression of these forcing terms is here omitted (see Ibrahim (2005) and Reclari (2013), among others, for a full derivation up to the second and third order). The bar denotes the complex conjugate. Also note that amplitude  $F$  is actually a real quantity and in the following the superscript  $\bar{F}$  will be used only to indicate forcing terms produced by the combination of the direct and complex conjugate contributions of the first order response to the external forcing. The r.h.s. of equation (3.11) clearly shows how second order terms naturally induce a superharmonic response, whose spatial periodicity is  $m = 2$ , hence precisely corresponding to the double-crest dynamics experimentally observed. The second forcing term on the r.h.s. of (3.11) has  $\omega = 0$  and  $m = 0$ , i.e. it is steady and axisymmetric. It originates in the leading order contribution in the time and azimuthal averaged flow, the so-called mean flow. Equation (3.11) was solved analytically by Reclari *et al.* (2014) by retaining for convenience only two modes, namely those with  $(m, n) = (2, 1)$  and  $(0, 1)$ , expected to

be the relevant ones. The numerical scheme employed in this work allows us to effortlessly account for all the  $(2, n)$  and  $(0, n)$  modes simultaneously, as their contribution will be directly encompassed in the spatial function  $\hat{\mathbf{q}}_2^{FF}$  and  $\hat{\mathbf{q}}_2^{F\bar{F}}$ , appearing in the second order solution,

$$\mathbf{q}_2 = \left( F^2 \hat{\mathbf{q}}_2^{FF} e^{i(2\Omega t - 2\theta)} + c.c. \right) + F^2 \hat{\mathbf{q}}_2^{F\bar{F}}, \quad (3.12)$$

whose contributions are computed by solving the following systems

$$(i2\Omega\mathcal{B} - \mathcal{A}_2) \hat{\mathbf{q}}_2^{FF} = \hat{\mathcal{F}}_2^{FF}, \quad -\mathcal{A}_0 \hat{\mathbf{q}}_2^{F\bar{F}} = \hat{\mathcal{F}}_2^{F\bar{F}} \quad (3.13)$$

The total flow field, obtained through the asymptotic model is then given by the sum of the first and second order solutions,

$$\mathbf{q} = \left( f \hat{\mathbf{q}}_1^F e^{i(\Omega t - \theta)} + f^2 \hat{\mathbf{q}}_2^{FF} e^{i(2\Omega t - 2\theta)} + c.c. \right) + f^2 \hat{\mathbf{q}}_2^{F\bar{F}}, \quad (3.14)$$

where, in order to eliminate the implicit small parameter  $\epsilon$ , the amplitudes  $\epsilon F$  and  $\epsilon^2 F^2$  are recast in terms of the physical amplitudes,  $f$  and  $f^2$ , respectively. The resulting prediction of the maximum crest-to-trough contact line amplitude,  $\delta(\theta, t) = \eta(r=1, \theta, t)$  is shown in figure 2 for driving frequencies close to  $\Omega/\omega_{21} \approx 0.5$  (see top-x-axis) as red solid lines. Although this straightforward asymptotic expansion detects the emergence of the super-harmonic double-crest wave in that frequency window, it completely fails in capturing the correct nonlinear wave amplitude saturation displaying a *hardening* behaviour clearly visible in figure 2. Once again, the amplitude of the inviscid second harmonic response is proportional to  $\propto 1/(\omega_{2n}^2 - 4\Omega^2)$  and the total solution tends to diverge close to the double-crest super-harmonic at  $\omega_{21}/2$ .

Such a close-to-resonance divergent behaviour is actually expected (particularly in absence of any form of dissipation) when performing straightforward asymptotic expansions, as they typically suffer from secular (or resonating) terms that must be properly treated (see Castaing (2005) and Nayfeh (2008) among many other references).

#### 4. Weakly nonlinear analysis via multiple timescale method

In order to overcome the aforementioned limitations of the straightforward asymptotic expansion procedure and thus to attempt to bridge the gap between theoretical predictions and experimental observations, we conduct in this section a weakly nonlinear analysis (WNL) based on the multiple timescale method. With the aim to derive a weakly nonlinear amplitude equation governing the double-crest dynamics (DC), we first tackle the simpler problem of single-crest waves (SC). In both cases we look for a third order asymptotic solution of the system

$$\mathbf{q} = \{\Phi, \eta\}^T = \epsilon \mathbf{q}_1 + \epsilon^2 \mathbf{q}_2 + \epsilon^3 \mathbf{q}_3 + \mathcal{O}(\epsilon^4), \quad (4.1)$$

where the zero order solution,  $\mathbf{q}_0 = \mathbf{0}$ , is omitted.

##### 4.1. Single-crest dynamics (SC)

In §3 the forcing amplitude  $f$  was assumed of order  $\epsilon$ , thus leading to a linear first order problem directly forced by the external shaking, which produces a divergent response close to harmonic resonances. With regards to single-crest waves and specifically to the harmonic response at a driving frequency close to that of one of the non-axisymmetric modes,  $\omega_{1n}$ , we assume here a small forcing amplitude of order  $\epsilon^3$ . This assumption is justified by the fact that close-to-resonance,  $\Omega \approx \omega_{1n}$ , and in absence of dissipation, even a small forcing will induce a large system response. The following analysis is therefore



expected to hold for  $\Omega = \omega_{1n} + \lambda$ , where  $\lambda$  is a small detuning parameter, here assumed of order  $\epsilon^2$ . Lastly, in the spirit of the multiple scale technique, we introduce the slow time scale  $T_2 = \epsilon^2 t$ , with  $t$  being the fast time scale at which the free surface oscillates with angular frequency  $\approx \omega_{1n}$ . Hence, the following scalings are assumed:

$$f = \epsilon^3 F, \quad \lambda = \epsilon^2 \Lambda, \quad T_2 = \epsilon^2 t, \quad (4.2)$$

We note that the forcing amplitude could be assumed of order  $\epsilon^2$  (as the other parameters), however this complicates unnecessarily the second order problem without modifying the final amplitude equation.

Although the asymptotic expansion is here pursued up to the third order in  $\epsilon$ , the procedure of the weakly nonlinear analysis is essentially equivalent to that of the straightforward asymptotic analysis discussed in §3. The major difference lies in the solution form of the leading order problem that is now a homogenous problem, as in equation (3.5). Given the azimuthal periodicity of the external forcing, among all possible natural eigenmodes we assume a leading order solution as

$$\mathbf{q}_1 = A_1(T_2) \hat{\mathbf{q}}_1^{A_1} e^{i(\omega_{1n} t - \theta)} + c.c., \quad (4.3)$$

where  $\hat{\mathbf{q}}_1^{A_1}$  is the eigenmode (computed by solving (3.5)) associated with  $(m, n) = (1, n)$  and  $\omega_{1n}$  is the corresponding natural frequency (solution of (3.6)).

The complex amplitude  $A_1$ , function of the slow time scale  $T_2$  and still unknown at this stage of the expansion, describes the slow time amplitude modulation of the oscillating wave  $\hat{\mathbf{q}}_1^{A_1}$  and introduces a new arbitrariness in the problem, which must be fixed at a higher order. Eigen-surface,  $\hat{\eta}_1^{A_1}$ , and eigen-potential field,  $\hat{\Phi}_1^{A_1}$ , computed for  $\omega_{1n} = \omega_{11}$ , are shown in figure 3(a) and (b), respectively.

By pursuing the expansion to the second order, a linear system forced by the first order solution and analogous to that of equation (3.11) is obtained (see Reclari (2013) for the full expansion of the original nonlinear governing equation up to the second order). Nevertheless, the forcing terms on the r.h.s. are here proportional to  $A_1^2$  (super- or second-harmonic) and to  $A_1 \bar{A}_1$  (mean flow). Thus, we seek for a second order solution of the form

$$\mathbf{q}_2 = A_1 \bar{A}_1 \hat{\mathbf{q}}_2^{A_1 \bar{A}_1} + \left( A_1^2 \hat{\mathbf{q}}_2^{A_1 A_1} e^{i(2\omega_{1n} t - 2\theta)} + c.c. \right), \quad (4.4)$$

with  $\hat{\mathbf{q}}_2^{A_1 \bar{A}_1}$  and  $\hat{\mathbf{q}}_2^{A_1 A_1}$  computed numerically and displayed in figure 3(c)-(d) and (e)-(f), respectively, in terms of second order free surface deformations and potential velocity fields evaluated for  $\omega_{1n} = \omega_{11}$ . From a numerical perspective, we note that the second order responses can be straightforwardly computed as long as the pairs  $(\omega, m) = (2\omega_{1n}, 2)$  and  $(0, 0)$  do not correspond to eigenvalues of (3.5), i.e. the second order operators  $(i2\omega_{1n} \mathcal{B} - \mathcal{A}_2)$  and  $-\mathcal{A}_0$  are non-singular and hence invertible.

With regards to figure 3, it is interesting to note how the second order mean flow potential velocity field is null everywhere. This can be rigorously proven by first noticing that the mean flow corresponds to a time- and azimuthal-averaged flow, i.e.  $\partial/\partial t = \partial/\partial \theta = 0$ . Moreover, in the inviscid limit, free surface elevation and potential field have a  $\pi/2$  phase shift, meaning that the first order eigenmode can be normalized such that the eigen-surface is purely real, whereas the eigen-potential is purely imaginary. Under these conditions, the mean flow forcing term on the r.h.s. of the kinematic equation cancels out, so that the associated Laplace equation appears to be constrained by homogeneous Neumann conditions on all the domain boundaries, thus prescribing a trivial constant potential field and therefore a null velocity field. In other words, the second order mean flow system reduces to forced linear meniscus equation (resulting from (2.3a)) and its

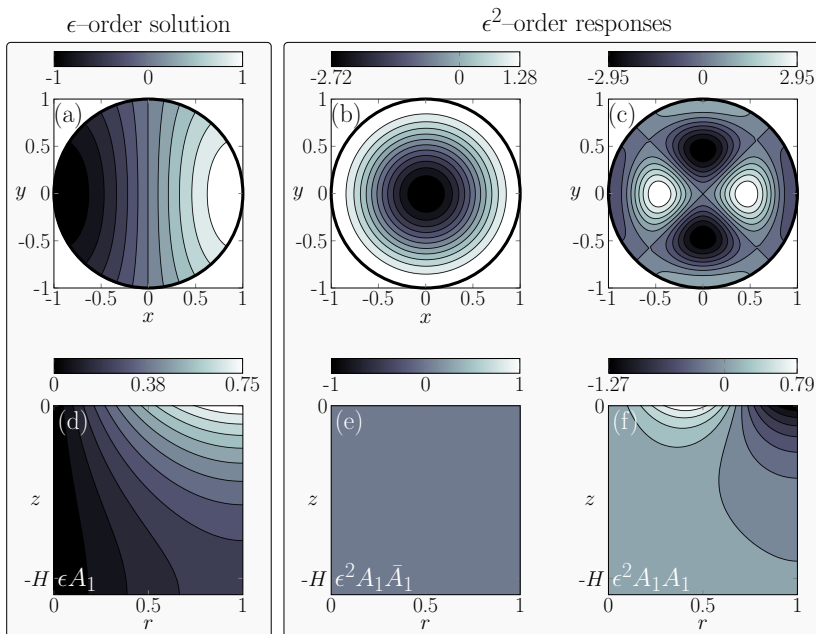


FIGURE 3. (a), (b) and (c): real part of the first,  $\hat{\eta}_1^{A_1}$ , and second order,  $\hat{\eta}_2^{A_1 A_1}$  and  $\hat{\eta}_2^{A_1 \bar{A}_1}$ , free surface deformations computed for  $\omega_{1n} = \omega_{11}$ . (d), (e) and (f): imaginary part of the associated first order,  $\hat{\phi}_1^{A_1}$ , and second order,  $\hat{\phi}_2^{A_1 A_1}$  and  $\hat{\phi}_2^{A_1 \bar{A}_1}$ , potential velocity field. Each response is denoted by its amplitude dependence,  $\epsilon A_1$ ,  $\epsilon^2 A_1 \bar{A}_1$  and  $\epsilon^2 A_1 A_1$ . The first order eigenmode is normalized with the amplitude and phase of the contact line (at  $r = 1$ ), such that the free surface,  $\hat{\eta}_1^{A_1}$  is purely real, whereas  $\hat{\phi}_1^{A_1}$  is purely imaginary. Note that the second order mean flow constantly induces an upside down *bell-like* axisymmetric interface deformation pushing the free surface downward at the center of the moving container. Calculations are performed for the case of figure 2, i.e. pure water with  $\rho = 1000 \text{ m/m}^3$ ,  $\gamma = 0.072 \text{ N/m}$ ,  $D = 0.287 \text{ m}$  and  $\tilde{H} = h/D = 0.52$ , for which  $Bo = 2802.8$  and  $\omega_{11} = 1.3286$ .

conditions at  $r = 0$  and  $r = 1$  (both  $\partial \hat{\eta}_2^{A_1 \bar{A}_1} / \partial r = 0$ ), which prescribes a static mean interface deformation only. Such a result was expected since the second order mean flow response represents the Eulerian mean flow, which, together with the so-called Stokes drift, contribute to the overall Lagrangian mean flow (see Bremer & Breivik (2018) for a thorough review). While the Stokes drift is a pure kinematic concept, the Eulerian mean flow, often referred to as streaming flow (Bouvard *et al.* 2017), is intrinsically a viscous concept. In other words, viscous boundary layers must be reintroduced if one aims to account for it.

We now move forward to the  $\epsilon^3$ -order problem, which is once again a linear problem forced by combinations of the first and second order solutions as well as by the slow time derivative of the leading order solution and by the external forcing, which was assumed of order  $\epsilon^3$ ,

$$\begin{aligned}
 (\partial_t \mathcal{B} - \mathcal{A}_m) \mathbf{q}_3 &= \mathcal{F}_3 = \quad (4.5) \\
 &= -\partial_{T_2} A_1 \mathcal{B} \hat{\mathbf{q}}_1^{A_1} e^{i(\omega_{1n} t - \theta)} + |A_1|^2 A_1 \hat{\mathcal{F}}_3^{A_1 \bar{A}_1 A_1} e^{i(\omega_{1n} t - \theta)} + F \hat{\mathcal{F}}_3^F e^{i\Lambda T_2} e^{i(\omega_{1n} t - \theta)} \\
 &\quad + \text{N.R.T.} + c.c.,
 \end{aligned}$$

with  $\hat{\mathcal{F}}_3^F = \{0, r/2\}^T$  and where N.R.T. stands for non-resonating terms, which are not relevant for further analysis. As standard in multiple scale analysis, the indeterminacy

introduced by the unknown amplitude  $A_1$  is resolved by requiring that secular terms do not appear in the solution to equation (4.5). Secularity results from all resonant forcing terms in  $\mathcal{F}_3$ , i.e. all terms sharing the same frequency and wavenumber  $(\omega_{1n}, 1)$  of  $\mathbf{q}_1$ , and in effect all terms explicitly written in (4.5). It follows that a compatibility condition must be enforced through the Fredholm alternative (Friedrichs 2012). Such a compatibility condition imposes the amplitude  $B = \epsilon A_1 e^{i\lambda t}$  to obey the following normal form

$$\frac{dB}{dt} = -i\lambda B + i\mu_{SC} f + i\nu_{SC} |B|^2 B, \quad (4.6)$$

where the physical time  $t = T_2/\epsilon^2$  has been reintroduced and where forcing amplitude and detuning parameter are recast in terms of their corresponding physical value,  $f = \epsilon^3 F$  and  $\lambda = \epsilon^2 A$ . Moreover, by considering that  $\mathbf{q} = \epsilon A_1 \hat{\mathbf{q}}_1^{A_1} + \dots$ , the small implicit parameter  $\epsilon$  is eliminated by defining the total physical amplitude  $A = \epsilon A_1$ . The subscript  $SC$  stands for single-crest (SC). The various normal form coefficients, which turn out to be real-valued quantities owing to the absence of dissipation, are computed as scalar products between the adjoint mode,  $\hat{\mathbf{q}}_1^{A_1\dagger}$ , associated with  $\hat{\mathbf{q}}_1^{A_1}$ , and the third order resonant forcing terms as follows

$$i\mu_{SC} = \frac{\langle \hat{\mathbf{q}}_1^{A_1\dagger}, \mathcal{B}\hat{\mathcal{F}}_3^F \rangle}{\langle \hat{\mathbf{q}}_1^{A_1\dagger}, \mathcal{B}\hat{\mathbf{q}}_1^{A_1} \rangle} = \frac{\int_{z=0} r \bar{\hat{\eta}}_1^{A_1\dagger} / 2 r dr}{\int_{z=0} \left( \hat{\eta}_1^{A_1\dagger} \hat{\Phi}_1^{A_1} + \hat{\Phi}_1^{A_1\dagger} \hat{\eta}_1^{A_1} \right) r dr}, \quad (4.7a)$$

$$i\nu_{SC} = \frac{\langle \hat{\mathbf{q}}_1^{A_1\dagger}, \mathcal{B}\hat{\mathcal{F}}_3^{A_1\bar{A}_1 A_1} \rangle}{\langle \hat{\mathbf{q}}_1^{A_1\dagger}, \mathcal{B}\hat{\mathbf{q}}_1^{A_1} \rangle} = \frac{\int_{z=0} \left( \hat{\eta}_1^{A_1\dagger} \hat{\mathcal{F}}_{3_{dyn}}^{A_1\bar{A}_1 A_1} + \hat{\Phi}_1^{A_1\dagger} \hat{\mathcal{F}}_{3_{kin}}^{A_1\bar{A}_1 A_1} \right) r dr}{\int_{z=0} \left( \hat{\eta}_1^{A_1\dagger} \hat{\Phi}_1^{A_1} + \hat{\Phi}_1^{A_1\dagger} \hat{\eta}_1^{A_1} \right) r dr}. \quad (4.7b)$$

Here  $\hat{\mathbf{q}}_1^{A_1\dagger} = \bar{\hat{\mathbf{q}}}_1^{A_1}$ , since the inviscid problem is self-adjoint with respect to the Hermitian scalar product  $\langle \mathbf{a}, \mathbf{b} \rangle = \int_{\Sigma} \bar{\mathbf{a}} \cdot \mathbf{b} dV$ , with  $\mathbf{a}$  and  $\mathbf{b}$  two generic vector (see Viola *et al.* (2018) for a thorough discussion and derivation of the adjoint problem). For the sake of brevity, the explicit expression of  $\hat{\mathcal{F}}_3^{A_1\bar{A}_1 A_1}$  is omitted, as it only involves straightforward calculations, i.e. a Taylor expansion of nonlinear governing equations and boundary conditions (2.2)-(2.3b) around the rest state  $\mathbf{q}_0 = \mathbf{0}$ . Here we simply denote with the subscript  $dyn$  and  $kin$  the forcing components appearing in the dynamic and kinematic boundary condition, respectively.

By turning to polar coordinates,  $B = |B|e^{i\Theta}$ , splitting the modulus and phase parts of (4.6) and looking for stationary solution,  $d/dt = 0$  with  $|B| \neq 0$ , the following implicit relation is obtained,

$$\tilde{d}_s \Omega^2 \mp \frac{(\lambda - \nu_{SC} |B|^2) |B|}{\mu_{SC}} = 0, \quad (4.8)$$

or, in a more common polynomial form,

$$P(|B|) = |B|^3 - \frac{\lambda}{\nu_{SC}} |B| \pm \frac{\mu_{SC} \tilde{d}_s \Omega^2}{\nu_{SC}} = 0, \quad (4.9)$$

where  $f = \tilde{d}_s \Omega^2$ ,  $\lambda = \Omega - \omega_{1n}$  and the  $\mp$  signs correspond to the phases  $\Theta = 0$  and  $\pi$ , respectively. The two branches described by (4.8) for  $|B|$  as a function of  $\Omega$  at a fixed non-dimensional shaking diameter  $\tilde{d}_s$  can be easily computed using the Matlab function *fimplicit*. After evaluating the stable and unstable stationary solutions for  $|B|$  and  $\Theta$ , the total single-crest wave solution is reconstructed as

---

$(m, n) \mid \tilde{H} = h/D \mid D \text{ [m]}$	$\omega_{mn}$	$\mu_{SC}$	$\nu_{SC}$
(1, 1)   0.50	0.287	$\omega_{11} = 1.3239$	0.27665 1.5265
(1, 2)   0.50	0.287	$\omega_{12} = 2.3206$	0.04189 17.0246
(1, 1)   0.52	0.287	$\omega_{11} = 1.3286$	0.27761 1.4847

---

TABLE 1. Value of the amplitude equation coefficient  $\mu_{SC}$  and  $\nu_{SC}$  in the conditions of figure 4.

---

$$\mathbf{q}_{SC} = \{\tilde{\Phi}, \eta\}^T = \mathbf{q}_1 + \mathbf{q}_2. \quad (4.10)$$

#### 4.1.1. Experiments vs weakly nonlinear prediction: wave amplitude

In figure 4(a) and (b) the weakly nonlinear (WNL) prediction in terms of maximum crest-to-trough contact line amplitude,  $\Delta\tilde{\delta}$ , for SC waves is compared with two sets of experimental measurements and with the potential linear solution (3.9). In comparison to the linear theory presented in §3, the agreement with experiments improves for different shaking diameters and for different harmonic resonances, e.g. those associated with modes  $(m, n) = (1, 1)$  and  $(1, 2)$  of figure 4(a). The *hardening* nonlinearity is correctly captured and the amplitude prediction matches well the measurements until the free surface eventually breaks and the wave regime leaves the weakly nonlinear regime, hence suggesting the little relevance of dissipative effects attributable to viscosity in this regime.

However, one must note that in this weakly nonlinear approach the driving frequency is essentially fixed around that of a unique non-axisymmetric natural mode,  $\Omega \approx \omega_{1n}$ . Consequently, when performing the analysis for a mode  $(1, n)$ , the influence of all other modes is completely overlooked. In consequence, the accuracy of the asymptotic solution rapidly deteriorates moving away from harmonic resonances, when compared to the linear solution (3.9), which turns out to be more accurate. This is visible looking at the bottom stable branch in the multi-solution range of figure 4(b) or by looking at the driving frequency window  $\Omega \in [0.7\omega_{12}, 0.9\omega_{12}]$  in figure 4(a). In other words, the detuning parameter should be small in order for the present weakly nonlinear analysis, based on a single mode expansion, to hold. On this regard, as no other natural frequencies are encountered for  $\Omega < \omega_{11}$ , an exception is made for the left branch associated with the harmonic resonance of the first (or fundamental) non-axisymmetric mode, where an excellent agreement of the single mode prediction, comparable to that of the linear solution, lasts until  $\Omega \approx 0$ , i.e. there is no need to employ a leading order multimodal expansion.

#### 4.1.2. The Duffing oscillator analogy

Mass-spring models are widely employed in several engineering fields, e.g. in aerospace engineering, for the description of close-to-resonance sloshing motions (Moiseev 1958; Bauer 1966; Dodge 2000), where nonlinearities are of crucial importance. The most popular driven nonlinear mass-spring model is that developed by Duffing (1918), who added a cubic nonlinear spring deformation (cubic term) to the classical driven harmonic oscillator

$$\ddot{x} + 2\sigma\dot{x} + x + c_3x^3 = p \cos \Omega t, \quad (4.11)$$

where  $\sigma$  is the damping coefficient and where, depending on the sign of  $c_3$  the resonance curve bends and the nonlinear resonance frequency shifts, i.e. it decreases for *softening*

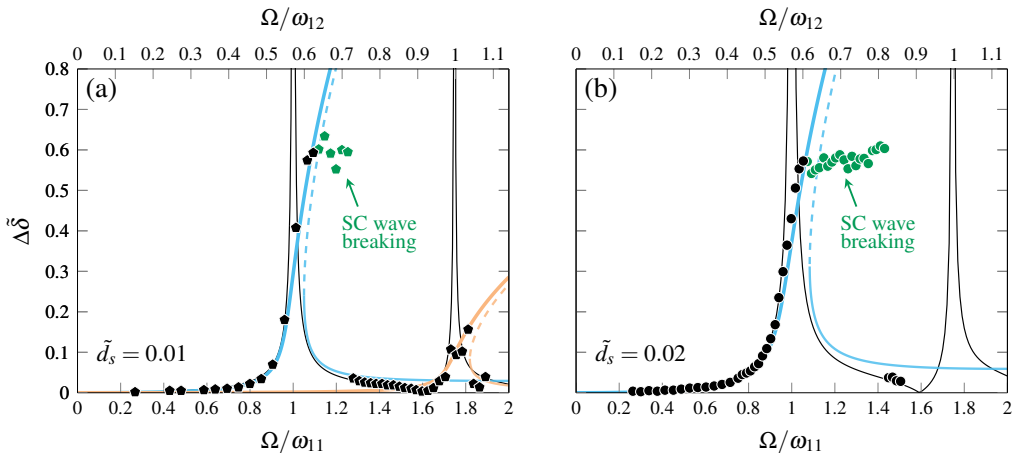


FIGURE 4. Comparison of the WNL-MTS prediction with experiments in terms of maximum crest-to-trough contact line amplitude (non-dimensional),  $\Delta\tilde{\delta}$ . (a) Black filled pentagons correspond to the experimental measurements presented by Reclari (2013) for  $\tilde{d}_s = d_s/D = 0.01$ ,  $\tilde{H} = h/D = 0.5$  and  $D = 0.287$  m, where the first two non-axisymmetric mode with  $(m, n) = (1, 1)$  and  $(1, 2)$  are detected. Solid black lines: solution of the linear potential model according to (3.9). Colored lines: WNL-MTS prediction (4.10). The unstable branch is represented as a dashed line. The values of normal form coefficient  $\mu_{SC}$  and  $\nu_{SC}$  computed for  $\Omega \approx \omega_{11}$  and  $\omega_{12}$  are given in table 1. (b) Same as (a) with the black filled circles corresponding to the case of figure 2 with  $\tilde{d}_s = 0.02$ ,  $\tilde{H} = 0.52$  and  $D = 0.287$  m and for mode  $(1, 1)$ ,  $\Omega \approx \omega_{11}$ .

spring ( $c_3 < 0$ ), whereas it increases for a *hardening* spring ( $c_3 > 0$ ), thus explaining the original observation of Duffing on vibration mechanism. Ockendon & Ockendon (1973) showed via asymptotic expansion of the potential flow solution in the neighborhood of a harmonic resonance that for small external forcing amplitudes, sloshing in a two-dimensional rectangular container responds exactly as an undamped Duffing oscillator (with  $\sigma = 0$ ). In Appendix B, we briefly show that, as expected, the same holds for close-to-harmonic-resonance sloshing in orbital shaken cylindrical containers, whose formal amplitude equation, starting from the full inviscid hydrodynamic system, was derived in §4.1 (see equation (4.6)). Typically, when the Duffing equation is employed to model close-to-resonance responses in sloshing dynamics and experimental measurements are available, the nonlinear coefficient is often computed by fitting the experimental measurements. Recently, with regards to quasi-two-dimensional rectangular containers laterally excited, Bäuerlein & Avila (2021) have carried out careful quantitative comparisons between experiments and theoretical predictions from the damped Duffing equation, showing that their actual sloshing system is remarkably well described by the forced-damped Duffing oscillator. Nevertheless, for increasing wave amplitude responses, experiments deviate from the Duffing solution, which is not capable to predict correctly the phase lag between driving and response, shown to be the key factor for an accurate estimation of the sloshing amplitude of the maximal nonlinear resonance (Bäuerlein & Avila 2021; Cenedese & Haller 2020). We note that, by analogy with the undamped Duffing equation, the weakly nonlinear analysis formalized in §4.1 exacerbates this aspect, since, owing to the lack of dissipation, it can only predict the classic phase lag bounds, 0 and  $\pi$  (see Appendix A for further comments on this regard). Nevertheless, one should notice that this intrinsic limitation turns to be unimportant in cases as those of figure 4, where for increasing amplitude a wave breaking eventually occurs and the weakly nonlinear theory

as well as the Duffing mechanical analogy no longer apply.

#### 4.2. Double-crest dynamics (DC)

We now tackle the double-crest (DC) wave response. Its formalization is slightly more subtle, as it requires a new reordering of the small control parameter magnitudes as well as an unusual form of the leading order problem, involving both a homogenous and a particular solution. We remind that the double-crest dynamics in figure 2 occurs at a driving frequency  $\Omega \approx \omega_{21}/2$ . Results at the end of this section will be presented for mode (2, 1), for which experiments are available, however, for the sake of generality, we formalize the analysis for any mode (2,  $n$ ), i.e.  $\Omega = \omega_{2n}/2 + \lambda$ , where  $\lambda$  is the detuning parameter.

##### 4.2.1. Formalism

To determine a suitable scaling for the forcing amplitude  $f$  and detuning parameter  $\lambda$  it is instructive to look at the experimental measurements shown in figure 2 for  $\Omega$  close to  $\omega_{21}/2$ . One can see that approaching  $\Omega \approx \omega_{21}/2$  from lower frequencies, the double-crest wave emerges on the top of a single-crest dynamics, i.e a single-to-double wave transition takes place, with the latter being correctly described by the linear solution, which still behaves well as  $\omega_{21}/2$  is far enough from the harmonic resonance occurring at  $\omega_{11}$ . It follows that the forcing amplitude  $f$  and detuning  $\lambda$  could be retained at order  $\epsilon$  and the first order problem takes the form (3.2), with  $\mathcal{F}_1 = F \{0, r/2\}^T e^{i(\Omega t - \theta)} + c.c. = F \hat{\mathcal{F}}_1^F e^{i(\omega_{2n}/2t - \theta)} e^{i\epsilon \Lambda t} + c.c.$ , with  $f = \epsilon F$  and  $\lambda = \epsilon \Lambda$ .

Furthermore, in §3 we have shown how, close enough to the super-harmonic resonance, the divergent behaviour is produced by a second order resonating term, which breaks the straightforward expansion, as  $\epsilon^2$ -order terms should not become larger than the  $\epsilon$ -order ones. In the following, this asymptotic breakdown is overcome by assuming that the leading order solution is given by the sum of (i) a particular solution, given by the linear response to the external forcing computed by solving (3.10), and (ii) a homogeneous solution, represented by the natural mode  $(m, n) = (2, n)$ , obtained by solving the generalized eigenvalue problem (3.5), up to an amplitude to be determined at higher orders. The second order resonating term will then require, in the spirit of multiple timescale analysis, an additional second order solvability condition, complementing the third order non-resonance condition already obtained in the single-crest wave weakly nonlinear model. This suggests that two slow time scales exist, namely  $T_1$  and  $T_2$ , with  $T_1$  one  $\epsilon$ -order faster than  $T_2$ , hence implying that quadratic nonlinearities are stronger than cubic ones. To summarize, the fundamental scalings underpinning the weakly nonlinear multiple scale expansion for double-crest waves are the following:

$$f = \epsilon F, \quad \lambda = \epsilon \Lambda, \quad T_1 = \epsilon t, \quad T_2 = \epsilon^2 t, \quad (4.12)$$

$$\mathbf{q}_1 = A_2(T_1, T_2) \hat{\mathbf{q}}_1^{A_2} e^{i(\omega_{2n}t - 2\theta)} + F \hat{\mathbf{q}}_1^F e^{i((\omega_{2n}/2)t - \theta)} e^{i\Lambda T_1} + c.c., \quad (4.13)$$

where the unknown slow time amplitude modulation,  $A_2$ , is here a function of the two time scales  $T_1$  and  $T_2$ , while the amplitude of the particular solution simply equals the forcing amplitude and  $\hat{\mathbf{q}}_1^F$  is computed from (3.10) for  $\Omega = \omega_{2n}/2$ .

The second order linearized forced problem reads

$$(\partial_t \mathcal{B} - \mathcal{A}_m) \mathbf{q}_2 = \mathcal{F}_2 = \mathcal{F}_2^{i,j} - \frac{\partial A_2}{\partial T_1} \mathcal{B} \hat{\mathbf{q}}_1^{A_2} e^{i(\omega_{2n}t - 2\theta)} - i\Lambda F \mathcal{B} \hat{\mathbf{q}}_1^{\Lambda F} e^{i((\omega_{2n}/2)t - \theta)} e^{i\Lambda T_1} + c.c.. \quad (4.14)$$

	$\epsilon A_2$	$\epsilon F$	$\epsilon^2 A_2 A_2$	$\epsilon^2 \Lambda F$	$\epsilon^2 A_2 \bar{A}_2$	$\epsilon^2 F \bar{F}$	$\epsilon^2 A_2 F$	$\epsilon^2 A_2 \bar{F}$
$\check{m}$	2	1	4	1	0	0	3	1
$\check{\omega}$	$\omega_{2n}$	$\omega_{2n}/2$	$2\omega_{2n}$	$\omega_{2n}/2$	0	0	$3\omega_{2n}/2$	$\omega_{2n}/2$

TABLE 2. First order linear solutions and second order non-resonating forcing terms gathered by their amplitude dependency and corresponding azimuthal and temporal periodicity  $(\check{m}, \check{\omega})$ . Six terms have been omitted as they are the complex conjugates of  $\epsilon A_2$ ,  $\epsilon F$ ,  $\epsilon^2 A_2 A_2$ ,  $\epsilon^2 F \bar{F}$ ,  $\epsilon^2 A_2 F$  and  $\epsilon^2 A_2 \bar{F}$ .

The first order solution is made of four different contributions of amplitude  $A_2$ ,  $\bar{A}_2$ ,  $F$  and  $\bar{F}$ , therefore it generates 10 different second order forcing terms, here denoted by  $\mathcal{F}_2^{i,j}$ , which exhibit a certain frequency and azimuthal periodicity,  $(\check{\omega}, \check{m})$ . The additional two forcing terms stem from the time-derivative of the first order solution (4.13) with respect to the first order slow time scale  $T_1$ . In order to interpret the last term in (4.14), it is worth first noting that, while the amplitude of the linear solution (3.9), computed at a generic driving frequency, grows with  $\Omega$  as  $F/(\omega_{11}^2 - \Omega^2) = \check{d}_s \Omega^2 / (\omega_{11}^2 - \Omega^2) \propto \Omega^2 / (\omega_{11}^2 - \Omega^2)$ , in the weakly nonlinear model for double-crest waves, the amplitude of the particular solution (4.13) is proportional to  $F/(\omega_{11}^2 - \omega_{21}^2/4) = \check{d}_s \Omega^2 / (\omega_{11}^2 - \omega_{21}^2/4) \sim \Omega^2$ , since the driving frequency was frozen at  $\Omega = \omega_{21} + \lambda$ , with the small detuning parameter,  $\lambda$ , contributing to modify its phase, but not its amplitude. This leads to an increasing discrepancy between (3.9) and the leading order particular solution (4.13) away from the super-harmonic resonance. The response to the forcing term proportional to  $\Lambda F$  in (4.14) can be then interpreted as a second order correction of the amplitude of the first order particular solution accounting for a detuning from the exact resonance through  $\Lambda F \propto \check{d}_s \Omega^2 (\Omega - \omega_{2n}/2)$  and contributing to improve the asymptotic approximation in a wider range of driving frequency in the neighbourhood of the super-harmonic frequency.

None of the forcing terms in (4.14) is resonant, as their oscillation frequency and azimuthal wavenumber differ from those of the leading order homogeneous solution, except the term produced by the second-harmonic of the leading order particular solution, i.e.  $\mathcal{F}_2^{FF} = F^2 \hat{\mathcal{F}}_2^{FF} e^{i(\omega_{2n} - 2\theta)} e^{i2\Lambda T_1} + c.c.$ . To avoid secular terms, a second order compatibility condition is imposed, requiring that the following normal form is verified

$$\frac{\partial A_2}{\partial T_1} = i \mu_{DC} F^2 e^{i2\Lambda T_1}, \quad (4.15)$$

with  $\mu_{DC}$  computed as before, i.e.

$$i \mu_{DC} = \frac{\int_{z=0} \left( \hat{\eta}_1^{A_2 \dagger} \hat{\mathcal{F}}_{2\text{dyn}}^{FF} + \hat{\Phi}_1^{A_2 \dagger} \hat{\mathcal{F}}_{2\text{kin}}^{FF} \right) r dr}{\int_{z=0} \left( \hat{\eta}_1^{A_2 \dagger} \hat{\Phi}_1^{A_2} + \hat{\Phi}_1^{A_2 \dagger} \hat{\eta}_1^{A_2} \right) r dr}, \quad (4.16)$$

Taken alone, the dynamics resulting from (4.15) is however of little relevance, since the solution, i.e. the frequency-response curve, would still diverge (symmetrically) to infinity for  $\Lambda = \Omega - \omega_{2n}/2 \rightarrow 0$  in absence of any restoring term, i.e. the nonlinear mechanism responsible for the finite amplitude saturation, which only comes into play at order  $\epsilon^3$ . This means that the expansion must be pursued up to the following order, and thereby that we must solve for the second-order solution.

By substituting (4.15) in the forcing expression, equation (4.14) can be rearranged as

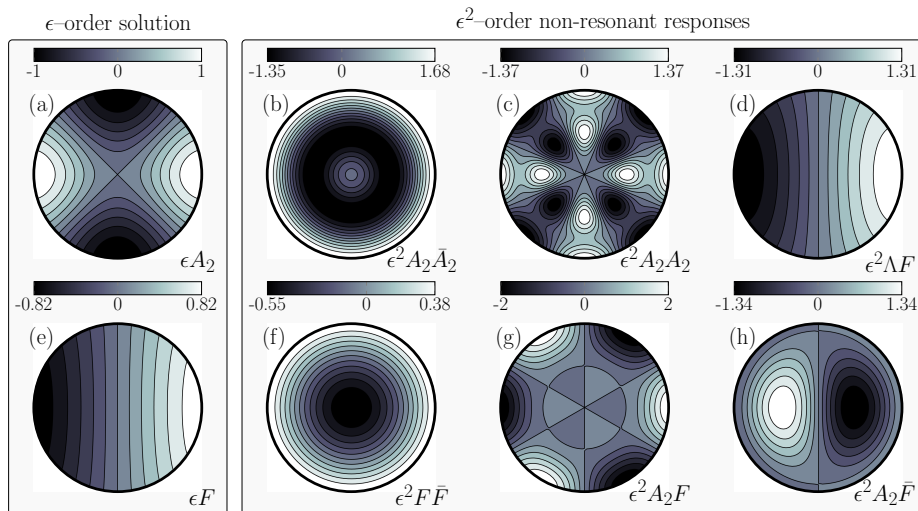


FIGURE 5. Real part of the first, (a)  $\hat{\eta}_1^{A_2}$  and (e)  $\hat{\eta}_1^F$ , and non-resonating second order, (b)  $\hat{\eta}_2^{A_1 \bar{A}_2}$ , (c)  $\hat{\eta}_2^{A_2 A_2}$ , (d)  $\hat{\xi}_2^{AF}$ , (f)  $\hat{\eta}_2^{F \bar{F}}$ , (g)  $\hat{\eta}_2^{A_2 F}$  and (h)  $\hat{\eta}_2^{A_2 \bar{F}}$ , free surface deformations computed for  $\omega_{2n} = \omega_{21}$ . The first order eigenmode is normalized with the amplitude and phase of the contact line (at  $r = 1$ ), such that the free surface,  $\hat{\eta}_1^{A_2}$  is purely real, whereas  $\hat{\phi}_1^{A_2}$  is purely imaginary. Note that the second order mean flow  $\hat{\eta}_2^{F \bar{F}}$  constantly induces an upside down *bell*-like an axisymmetric interface deformation pushing the free surface downward at the center of the moving container, by analogy with the effect produced by  $\hat{\eta}_2^{A_1 \bar{A}_1}$  for SC waves, as the two responses are essentially equivalent up to a pre factor. Here the mean flow  $\hat{\eta}_2^{A_2 \bar{A}_2}$  for DC pushes the interface upward at the wall (same as  $\hat{\eta}_2^{F \bar{F}}$ ) and, at the same time, downward in an annular region at intermediate radial coordinates, without altering the free surface elevation at the container revolutions axis.

follows

$$\begin{aligned}
 (\partial_t \mathcal{B} - \mathcal{A}_m) \mathbf{q}_2 &= \mathcal{F}_{2_{NRT}}^{i,j} + \mathcal{F}_{2_{RT}}^{i,j} = \\
 &= \mathcal{F}_{2_{NRT}}^{i,j} + F^2 \left( \hat{\mathcal{F}}_2^{F \bar{F}} - i \mu_{DC} \mathcal{B} \hat{\mathbf{q}}_1^{A_2} \right) e^{i(\omega_{2n} t - 2\theta)} e^{i2AT_1} + c.c.,
 \end{aligned} \tag{4.17}$$

where the subscripts  $NRT$  and  $RT$  denote non-resonating (whose frequencies and azimuthal periodicities are gathered in table 2) and resonating terms, respectively. Note that the term proportional to  $\Lambda F$  has been included in the non-resonating forcing terms, whereas the resonant term is written explicitly. The compatibility condition is now trivially satisfied, meaning that the new forcing term is orthogonal to the adjoint mode,  $\hat{\mathbf{q}}_1^{A_2 \dagger} = \overline{\hat{\mathbf{q}}_1^{A_2}}$ , by construction and therefore, according to the Fredholm alternative, a non-trivial solution exists. Hence, we seek for a second order solution having the following form

$$\begin{aligned}
 \mathbf{q}_2 &= A_2 \bar{A}_2 \hat{\mathbf{q}}_2^{A_2 \bar{A}_2} + F^2 \hat{\mathbf{q}}_2^{F \bar{F}} + \\
 &+ A_2^2 \hat{\mathbf{q}}_2^{A_2 A_2} e^{i(2\omega_{2n} t - 4\theta)} + \Lambda F \hat{\mathbf{q}}_2^{AF} e^{i((\omega_{2n}/2)t - \theta)} e^{iAT_1} + \\
 &+ A_2 F \hat{\mathbf{q}}_2^{A_2 F} e^{i((3\omega_{2n}/2)t - 3\theta)} e^{iAT_1} + A_2 \bar{F} \hat{\mathbf{q}}_2^{A_2 \bar{F}} e^{i((\omega_{2n}/2)t - \theta)} e^{-iAT_1} + \\
 &+ F^2 \hat{\mathbf{q}}_2^{F \bar{F}} e^{i(\omega_{2n} t - 2\theta)} e^{i2AT_1} + c.c..
 \end{aligned} \tag{4.18}$$

All non-resonant responses in (4.18) are handled similarly, i.e. they are computed in Matlab by performing a simple matrix inversion using standard LU solvers (as in §§3 and 4.1). As anticipated above, although the operator associated with the resonant forcing



term, i.e.  $(i\omega_{2n}\mathcal{B} - \mathcal{A}_2)$ , is singular, the value of the normal form coefficient (4.16) ensures that a non-trivial solution for  $\hat{\mathbf{q}}_2^{FF}$  exists. Diverse approaches can be followed to compute this response. Here such a response is computed by using the *pseudoinverse* matrix of the singular operator (Orchini *et al.* 2016). Another possible approach is given in Appendix A of Meliga *et al.* (2012), where a two-step regularization procedure, involving an intermediate factious solution for  $\hat{\mathbf{q}}_2^{FF}$  is employed. We also note that in (4.18), exactly as in (4.4), a second order homogeneous solution has not been accounted for as its introduction would be irrelevant to the final solution.

The first order solutions together with all the non-resonating second order responses are shown in the various panels of figure 5, where the two leading order contributions,  $\epsilon A_2$  and  $\epsilon F$ , corresponding to the double- and single-crest wave, respectively, can be identified. Moreover, we note that the second order response proportional to  $\epsilon^2 \Lambda F$  has a spatial structure similar to that of the leading order response  $\epsilon F$ , as it represents the second order correction to the latter caused by small frequency shifts of order  $\epsilon$ .

Lastly, at third order in  $\epsilon$ , the problem reads

$$\begin{aligned} (\partial_t \mathcal{B} - \mathcal{A}_m) \mathbf{q}_3 &= \mathcal{F}_3 = & (4.19) \\ &= -\frac{\partial A_2}{\partial T_2} \mathcal{B} \hat{\mathbf{q}}_1^{A_2} e^{i(\omega_{2n}t - 2\theta)} - i2\Lambda F^2 \mathcal{B} \hat{\mathbf{q}}_2^{FF} e^{i(\omega_{2n}t - 2\theta)} e^{i2\Lambda T_1} + \\ &+ |A_2|^2 A_2 \hat{\mathcal{F}}_3^{A_2 \bar{A}_2 A_2} e^{i(\omega_{2n}t - 2\theta)} + A_2 F^2 \hat{\mathcal{F}}_3^{A_2 F \bar{F}} e^{i(\omega_{2n}t - 2\theta)} + \\ &+ \Lambda F^2 \hat{\mathcal{F}}_3^{A F F} e^{i(\omega_{2n}t - 2\theta)} e^{i2\Lambda T_1} + \text{N.R.T.} + c.c., \end{aligned}$$

where the first two forcing terms arise from the time-derivative of the first order solution with respect to the second order slow time scale  $T_2$  and from that of the second order solution with respect to the first order slow time scale  $T_1$ , respectively. By noticing that the second and last forcing terms share the same amplitude dependence, i.e.  $\Lambda F^2$ , they can be recast into a single forcing term, say  $\Lambda F^2 \hat{\mathcal{F}}_3^{A F F} e^{i(\omega_{2n}t - 2\theta)} e^{i2\Lambda T_1} + c.c.$ .

Once again, all terms explicitly written in (4.19) are resonant, as they share the same pair  $(\omega_{2n}, 2)$  than the first order homogeneous solution, hence a third order compatibility condition, leading to the following normal form, must be enforced

$$\frac{\partial A_2}{\partial T_2} = i\zeta_{DC} \Lambda F^2 e^{i2\Lambda T_1} + i\chi_{DC} A_2 F^2 + i\nu_{DC} |A_2|^2 A_2, \quad (4.20)$$

with

$$i\zeta_{DC} = \frac{\int_{z=0} \left( \hat{\eta}_1^{A_2 \dagger} \hat{\mathcal{F}}_{3_{\text{dyn}}}^{A F F} + \hat{\phi}_1^{A_2 \dagger} \hat{\mathcal{F}}_{3_{\text{kin}}}^{A F F} \right) r dr}{\int_{z=0} \left( \hat{\eta}_1^{A_2 \dagger} \hat{\phi}_1^{A_2} + \hat{\phi}_1^{A_2 \dagger} \hat{\eta}_1^{A_2} \right) r dr}, \quad (4.21a)$$

$$i\chi_{DC} = \frac{\int_{z=0} \left( \hat{\eta}_1^{A_2 \dagger} \hat{\mathcal{F}}_{3_{\text{dyn}}}^{A_2 F \bar{F}} + \hat{\phi}_1^{A_2 \dagger} \hat{\mathcal{F}}_{3_{\text{kin}}}^{A_2 F \bar{F}} \right) r dr}{\int_{z=0} \left( \hat{\eta}_1^{A_2 \dagger} \hat{\phi}_1^{A_2} + \hat{\phi}_1^{A_2 \dagger} \hat{\eta}_1^{A_2} \right) r dr}, \quad (4.21b)$$

$$i\nu_{DC} = \frac{\int_{z=0} \left( \hat{\eta}_1^{A_2 \dagger} \hat{\mathcal{F}}_{3_{\text{dyn}}}^{A_2 \bar{A}_2 A_2} + \hat{\phi}_1^{A_2 \dagger} \hat{\mathcal{F}}_{3_{\text{kin}}}^{A_2 \bar{A}_2 A_2} \right) r dr}{\int_{z=0} \left( \hat{\eta}_1^{A_2 \dagger} \hat{\phi}_1^{A_2} + \hat{\phi}_1^{A_2 \dagger} \hat{\eta}_1^{A_2} \right) r dr}. \quad (4.21c)$$

As a last step in the derivation of the final amplitude equation for the double-crest (DC) waves and in order to eliminate the implicit small parameter  $\epsilon$ , we unify (4.15) and (4.20) into a single equation recast in terms of the physical time  $t = T_1/\epsilon = T_2/\epsilon^2$ , physical forcing control parameters,  $f = \epsilon F$  and  $\lambda = \epsilon \Lambda$ , and total amplitude,  $A = \epsilon A_2$ . This

is achieved by summing (4.15) and (4.20) along with their respective weights  $\epsilon^2$  and  $\epsilon^3$ , thus obtaining

$$\frac{dB}{dt} = -i(2\lambda - \chi_{DC}f^2)B + i(\zeta_{DC}\lambda + \mu_{DC})f^2 + i\nu_{DC}|B|^2B, \quad (4.22)$$

where the change of variable  $A = Be^{i2\lambda t}$  has been introduced for convenience. As in §4.1, by turning to polar coordinates,  $B = |B|e^{i\theta}$ , splitting the modulus and phase parts of (4.22) and looking for stationary solution,  $d/dt = 0$  with  $|B| \neq 0$ , the following implicit relation is obtained,

$$\tilde{d}_s\Omega^2 - \sqrt{(2\lambda - \nu_{DC}|B|^2)|B|/[\chi_{DC}|B| \pm (\zeta_{DC}\lambda + \mu_{DC})]} = 0, \quad (4.23)$$

where only the real solutions corresponding to  $f = \tilde{d}_s\Omega^2 > 0$  are retained, as the combinations  $\tilde{d}_s\Omega^2 < 0$  are not physically meaningful.

Although two more terms appear in (4.22) and the dependence on the forcing amplitude is different with respect to the SC case, i.e.  $f^2$  instead of  $f$ , thus leading to the square root in (4.23), amplitude equation (4.22) is reminiscent of that given in (4.6). Indeed, equation (4.22) contains essentially three contributions,

$$\lambda \leftrightarrow (2\lambda - \chi_{DC}f^2), \quad \mu_{SC}f \leftrightarrow (\zeta_{DC}\lambda + \mu_{DC})f^2, \quad \nu_{SC} \leftrightarrow \nu_{DC}, \quad (4.24)$$

in order, a detuning term (forcing amplitude dependent), an additive (quadratic) forcing term (forcing frequency dependent) and the classic cubic restoring term, respectively. Hence, the same qualitative *hardening* or *softening* nonlinear behaviours as well as hysteresis, typical features of the Duffing-equation, are expected under the hypotheses of the present analysis.

The total flow solution predicted by the WNL for DC waves and reconstructed as

$$\mathbf{q}_{DC} = \{\Phi, \eta\}^T = \mathbf{q}_1 + \mathbf{q}_2, \quad (4.25)$$

is compared in figures 6 and 7 with experiments from Reclari (2013) and Reclari *et al.* (2014) (see also figure 2).

#### 4.2.2. Experiments vs weakly nonlinear prediction: wave amplitude

In figures 6 and 7, the weakly nonlinear (WNL) prediction of double-crest (DC) waves is quantitatively compared with the experimental measurements from Reclari (2013) and Reclari *et al.* (2014) in terms of maximum non-dimensional crest-to-trough contact line amplitude,  $\Delta\tilde{\delta}$ , for different values of the shaking diameters,  $\tilde{d}_s$  corresponding to those of figure 2 in the frequency window close to  $\omega_{21}/2$ .

The improvement gained through the formal WNL analysis, when compared with the linear and straightforward asymptotic models, is striking. The amplitude equation model correctly predicts the transition from a single- to a double-crest wave and the resulting finite amplitude saturation via *hardening* nonlinear mechanism, thus remarkably narrowing the gap with experiments for all the values of  $\tilde{d}_s$  considered and for different container configurations.

Notwithstanding such an improvement, figure 6 highlights the main limitation of the present amplitude equation model for DC waves. Indeed, one notices that, while at larger shaking diameters, i.e.  $\tilde{d}_s = 0.13$  and  $0.20$ , a DC wave first emerges on the top a single-crest (SC) dynamics and eventually a double-crest wave breaking occurs at larger frequencies, a jump-down transition from DC to SC takes place by increasing  $\Omega$  at lower shaking diameters, i.e.  $\tilde{d}_s = 0.07$  and  $0.10$  for  $D = 0.144$  m. This well-known hysteretic behaviour can be reasonably ascribed to the viscous dissipation of the system. For instance, at sufficiently small shaking diameters, e.g.  $\tilde{d}_s \approx 0.02$  (see figure 2), the DC

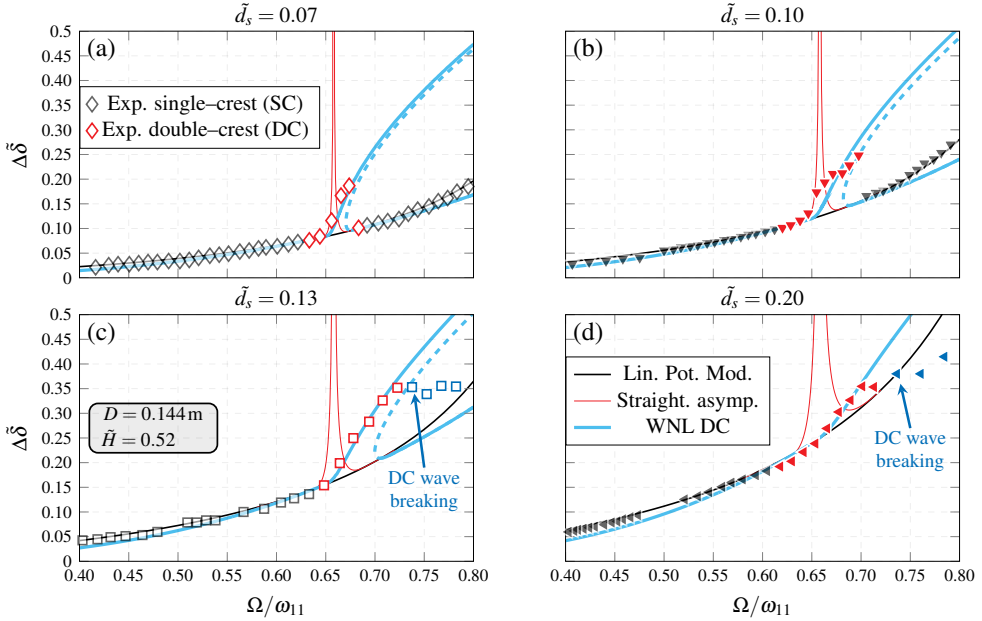


FIGURE 6. Weakly nonlinear (WNL) prediction for double-crest (DC) waves versus experiments by Reclari *et al.* (2014) (reported in figure 2 of this paper) in terms  $\Delta\tilde{\delta}$  for the smallest container diameter  $D = 0.144$  m, for different shaking diameters and at a driving frequency close to  $\Omega \approx \omega_{21}/2$  ( $\Omega/\omega_{11} = 0.6576$ ). Solid black lines: linear potential solution (3.9). Red solid lines: straightforward asymptotic solution (3.14). Light blue solid and dashed lines: stable and unstable branches, respectively, predicted by the WNL via (4.23). The normal form coefficient values for this configurations are  $\chi_{DC} = 3.4572$ ,  $\zeta_{DC} = 0.8708$ ,  $\mu_{DC} = 0.1292$  and  $\nu_{DC} = 10.0181$ .

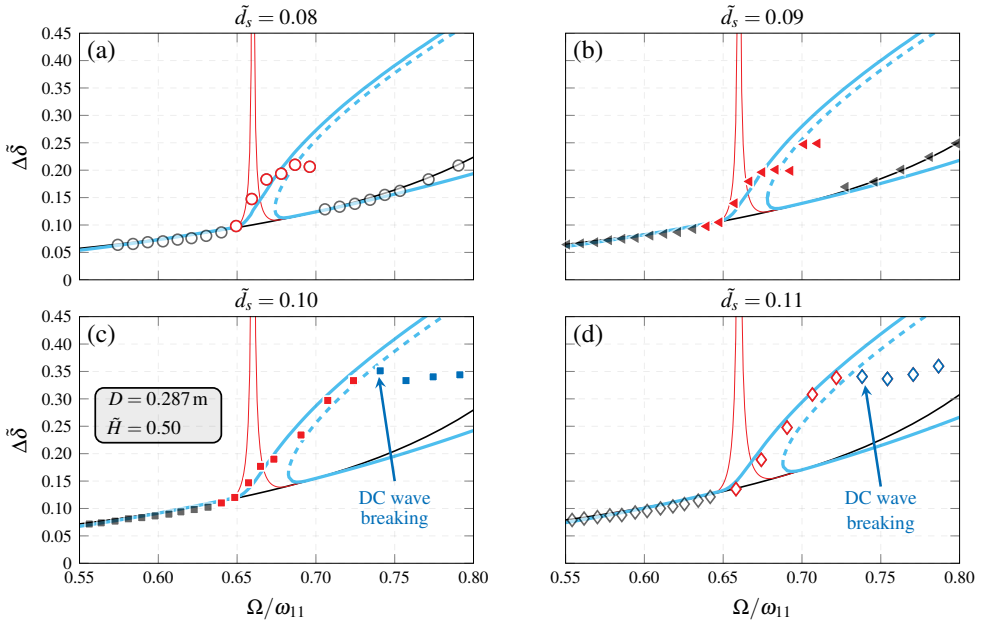


FIGURE 7. Same as figure 6 but for the largest container diameter  $D = 0.287$  m and  $\tilde{H} = 0.50$  (see figure 4.19 of Reclari (2013)). The normal form coefficient values for this configurations are  $\chi_{DC} = 3.4718$ ,  $\zeta_{DC} = 0.9059$ ,  $\mu_{DC} = 0.1338$  and  $\nu_{DC} = 9.8847$ .

dynamics does not manifest at all, as the energy pumped into the system by the external forcing is likely not sufficient to dominate over the system viscous dissipation, whose effect also depends on the container diameter,  $D$ . Indeed, figure 7 clearly shows that larger diameters, i.e.  $D = 0.287$  m, generate less dissipation. It follows that for larger  $D$ , by increasing the driving frequency at a fixed shaking diameter, e.g.  $\tilde{d}_s = 0.10$ , the free surface is more likely to undergo a wave breaking, rather than a jump-down transition (see figures 6(b) and 7(c)). Obviously, the inviscid model employed here is not capable to predict the so-called jump-down frequency. In Appendix A, a heuristic viscous damping model is introduced to tentatively overcome the beforehand mentioned limitations.

Finally, we note that, for frequency moderately far from the super-harmonic resonance, the agreement of the WNL model with experiments and with the linear solution, which behaves well away from  $\Omega \approx \omega_{11}$ , progressively deteriorates. This is particularly evident on the right stable branch and can be ascribed to the fact that the asymptotic model is essentially formalized for a fixed driving frequency, i.e.  $\Omega \approx \omega_{21}/2$ , thus filtering out the existence of other resonances. Nevertheless, owing to the assumption of detuning parameter of order  $\epsilon$ , the second order correction to the leading order particular solution guarantees a fairly good agreement in a relatively wide range of frequency around  $\omega_{21}/2$ .

#### 4.2.3. Experiments vs weakly nonlinear prediction: free surface reconstruction

In figure 8, the weakly nonlinear (WNL) models for the double-crest waves (DC) is compared versus the straightforward asymptotic prediction discussed in §3 and the experimental measurements for DC waves from Reclari (2013) and Reclari *et al.* (2014). The direct quantitative comparison is here outlined in terms of dimensionless and phase-averaged wave height measured at the sidewall,  $\tilde{\delta}(\theta)$ .

We observe that, if at  $\Omega/\omega_{21} = 0.490$  both models match satisfactorily the experimental points, as soon as  $\Omega/\omega_{21} = 0.5$  is approached, the straightforward asymptotic solution diverges due to the resonant (second order) super-harmonic term, while the WNL solution predicts correctly the finite amplitude saturation and the emergence of a DC wave on the top of a single-crest (SC) one. The WNL model for DC waves remains in fairly good agreement even at larger driving frequency, although the increasing phase-asymmetry between the two local peaks at  $\theta = \pi/2$  and  $3\pi/2$  is not retrieved by the present inviscid asymptotic analysis, where secondary effects, e.g. the phase shift induced by viscous dissipation and influence of other higher modes, as well as stronger nonlinear effects for increasing wave amplitudes are overlooked.

For completeness, the three-dimensional free surface,  $\eta(r, \theta, \pi/\Omega)$ , is reconstructed through (4.25) and shown in the right-panels of figure 8, where, for increasing shaking frequencies, the nonlinear transition from a nearly single-crest wave dynamics to a double-crest wave dynamics is enlightened.

#### 4.2.4. The Helmholtz–Duffing oscillator analogy

While the Duffing equation is known to capture period-3 and period-1/3 dynamics arising from the cubic nonlinearity (Jordan & Smith 1999; Kalmár-Nagy & Balachandran 2011), as those observed by Bäuerlein & Avila (2021) and occasionally by Reclari *et al.* (2014), it cannot predict the period-halving dynamics associated with the super-harmonic resonance investigated in this paper. Therefore, in connection with §4.1.2, here we aim to identify the simplest possible mechanical oscillator that could mimic, at least from a qualitative perspective, the period-1/2 dynamics studied in this work.

The weakly nonlinear analysis (WNL) as well as the straightforward asymptotic model highlighted the crucial role of quadratic nonlinearities emerging at second order and from which the double-crest (DC) dynamics stems. At the same time, the WNL model

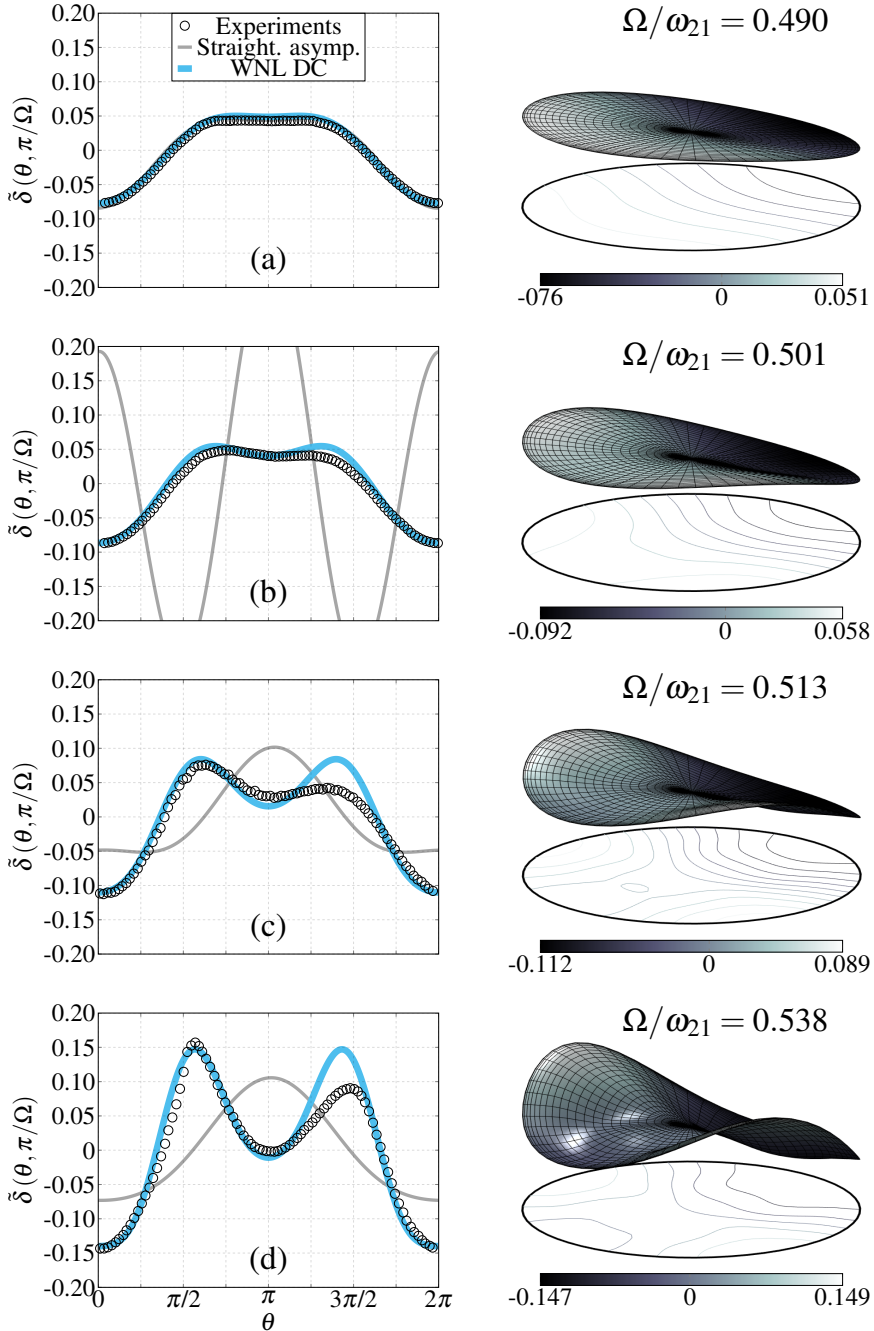


FIGURE 8. Left-panels: comparison of the dimensionless and phase-averaged wave height measured at the wall,  $\tilde{\delta}(\theta, \pi/\Omega)$ , (black circles) with the straightforward asymptotic solution rebuilt via (3.14) (gray solid line) and the weakly nonlinear (WNL) solution for the double-crest (DC) wave (4.25). Panels correspond to  $\tilde{H} = 0.52$ ,  $\tilde{d}_s = 0.11$  and  $D = 0.144$  m. The experimental measurements, here shown as black circles, are available in Reclari (2013), except for panel (c), which is provided in Reclari *et al.* (2014). Note that (b) the nonlinear prediction has a very large amplitude. Right-panels: corresponding three-dimensional free surface deformation,  $\eta(r, \theta, \pi/\Omega)$ , reconstruct via (4.25). The single-to-double crest transition via hardening nonlinearity is clearly visible moving from top to bottom, i.e. for increasing frequency.

enlightened that second order terms only are not sufficient to capture all the dynamics features owing to the lack of restoring terms and, therefore, cubic nonlinearities must be retained. These considerations suggest that the DC dynamics could be tentatively described by a driven oscillator with both quadratic (asymmetric) and cubic (symmetric) nonlinear terms, i.e.

$$\ddot{x} + 2\sigma\dot{x} + x + c_2x^2 + c_3x^3 = p \cos \Omega t. \quad (4.26)$$

Equation (4.26), also commonly known as Helmholtz–Duffing equation, has wide applications in engineering problems as those related to beams, plates and shells subjected to an initial static curvature (Mirzabeigy *et al.* 2014; Askari *et al.* 2011), whose governing equations are reconduced to a second-order nonlinear ordinary equation with quadratic and cubic nonlinear terms (Ke *et al.* 2010; Alijani *et al.* 2011; Fallah & Aghdam 2011).

Among the diverse asymptotic solutions of (4.26) in different limits (Rega 1995; Benedettini & Rega 1989; Kovacic & Brennan 2011), the most relevant to our work is that of Benedettini & Rega (1989). Within the context of planar nonlinear response of suspended elastic cables to an external excitation, they derived an amplitude equation which concerns with the first or fundamental super-harmonic excitation, i.e.  $\Omega \approx 1/2$ , of (4.26). Their weakly nonlinear approach is detailed in Appendix C, with the additional assumption of vanishing damping  $\sigma = 0$ . Assuming  $2\Omega = 1 + \lambda = 1 + \epsilon\hat{\lambda}$ , small nonlinearities,  $c_2 = \epsilon\hat{c}_2$  and  $c_3 = \epsilon^2\hat{c}_3$ , and introducing two slow time scales, one obtains

$$dD/dt = -i(\lambda + c_5f^2)D + i(1 - \lambda/2)c_2f^2/2 - i4c_4|D|^2D, \quad (4.27)$$

with  $C = De^{i\lambda t}$  and with the auxiliary coefficients  $c_4$  and  $c_5$  (both functions of  $c_2$  and  $c_3$ ) defined in Benedettini & Rega (1989). By comparing term by term, the analogy with equation (4.22) is evident.

To conclude, although the DC dynamics examined in this paper is intrinsically related to the simultaneous interplay of multiple waves, thus making particularly challenging an accurate *vis-à-vis* quantitative comparison with a single-degree-of-freedom mechanical model, equation (4.27) seems to suggest that the actual inviscid sloshing dynamics in the DC regime may be, at least qualitatively, described by the undamped Helmholtz–Duffing equation (4.26) driven super-harmonically.

## 5. Conclusion

With regards to orbital shaken cylindrical containers and, specifically, to the careful experimental campaign reported in Reclari (2013) and Reclari *et al.* (2014), a weakly nonlinear analysis (WNL) via multiple timescale method was formalized in §4 in order to investigate diverse features of the steady state free surface dynamics and, particularly, the double-crest (DC) wave dynamics pertaining at half the frequency of the first  $m = 2$  natural mode.

After having discussed the substantial limitations of the straightforward expansion procedure propose by Reclari *et al.* (2014) and summarized in §3, the WNL analysis was first formulated under the most common condition of pure harmonic resonance. Despite the inviscid assumption, the WNL analysis developed for the single-crest (SC) wave dynamics was shown to be in fairly good agreement with all the experimental measurements. In fact, the present model correctly describes the close-to-resonance *hardening* nonlinear behaviour experimentally observed. The agreement remains sufficiently accurate until the free surface eventually breaks and a transition to a fully nonlinear regime occurs.

It is well-assessed in the literature that the close-to-harmonic-resonance sloshing dynamics can be modeled (from both qualitative and quantitative perspectives (Bäuerlein

& Avila 2021)) by a single degree of freedom (1dof) system with a cubic nonlinearity and driven harmonically, i.e. by the famous Duffing oscillator, as rigorously proved for a two-dimensional rectangular container laterally excited (Ockendon & Ockendon 1973). Without surprise, this was shown to hold for the case of orbital shaken cylindrical containers as well.

The WNL analysis was then extended to the more complex case of a double-crest wave dynamics and to the resulting single-to-double crest wave transition. The overall agreement with experiments and, especially, the improvements with respect to the simple straightforward asymptotic model are remarkable in all cases considered, although the slight asymmetry observed in the reconstruction of the periodic free surface dynamics at the sidewall was not retrieved in the present model.

To the knowledge of the authors, a formal amplitude equation describing the super-harmonic DC sloshing dynamics in orbital shaken containers and coupled with a thorough experimental validation, has not been reported in the literature yet, hence representing the most significant finding of this work.

Lastly, by analogy with the close-to-harmonic-resonance dynamics for SC waves, for which the Duffing oscillator represent the suitable mechanical analogy, a one-degree-of-freedom (1dof) mechanical oscillator having both quadratic and cubic nonlinear terms, commonly referred to as Helmholtz-Duffing (HD) oscillator, driven super-harmonically, was tentatively identified as the simplest possible mechanical system that could mimic, at least qualitatively, the super-harmonic DC sloshing dynamics investigated in this paper. The HD equation was largely adopted in the last few decades within the context of structural analysis, i.e. beams, plates and shells subjected to an initial static curvature as well as suspended elastic cables (Nayfeh 1984; Benedettini & Rega 1989), and it was here proposed as direct mechanical analogy with the present orbital sloshing system.

The main limitation of the models derived in this work is intrinsic to the fundamental assumption of an inviscid fluid. This precludes one to correctly account for the jump-down transition experimentally observed for DC waves at low shaking amplitudes and, therefore, for an accurate estimation of the maximum amplitude response when such a transition occurs. Furthermore, in absence of viscous boundary layers, the weakly nonlinear time- and azimuthal-averaged mean flow reduces to a free surface deformation only. This is in stark contrast with existence of the so-called Eulerian mean flow (Bremer & Breivik 2018), also known as viscous streaming flow, typically observed in experiments (Bouvard *et al.* 2017). Therefore, the present work overlooks one of the essential points of interest in applications of orbital shaking. The mean flow, which contributes to an efficient mixing, is not captured.

The extension of the asymptotic models developed in this work to a viscous analysis is desirable, as it would enable one to predict quantitatively these secondary but fundamental effects for both cases of harmonic and super-harmonic resonances. However, it presently hinges on the subtle modeling of the moving contact line condition.

## Appendix A. Heuristic damping model: jump-down frequency and DC dynamics suppression at low driving amplitudes

In §4.2.2 the weakly nonlinear (WNL) model for double-crest (DC) waves was compared with experimental measurements from Reclari (2013) and Reclari *et al.* (2014) in terms non-dimensional maximum crest-to-trough contact line amplitude,  $\Delta\tilde{\delta}$ , for different non-dimensional shaking diameters,  $\tilde{d}_s$ , and container diameters,  $D$  (see figures 6 and 7). We have observed that at larger shaking amplitudes,  $\tilde{d}_s$ , and for larger container diameter,  $D$ , a DC wave first emerges on the top of a single-crest (SC) wave at  $\Omega \approx \omega_{21}/2$  and

eventually wave breaking occurs at larger frequencies. On the contrary, a jump-down transition from DC to SC then takes place by increasing  $\Omega$  at lower values of  $\tilde{d}_s$  and/or for smaller  $D$ . The latter well-known hysteretic behaviour can be ascribed to the viscous dissipation of the system, obviously overlooked by the present inviscid analysis. In this Appendix, viscous dissipation is tentatively reintroduced by employing a simple heuristic viscous damping model, as described in the following.

The viscous dissipation essentially arises at three locations, (i) at the solid tank boundary layers, i.e. bottom and sidewall, (ii) in the fluid bulk and (iii) at the free surface, the latter being typically negligible for ideal surface waves (in absence of any form of contamination). A well-known formula for the prediction of the viscous damping coefficient of capillary-gravity waves in upright cylindrical containers was provided by Case & Parkinson (1957) and Miles (1967). Such an estimation is computed according to the following formula

$$\sigma = \frac{2k_{mn}}{Re} + \left(\frac{\omega_{mn}}{2Re}\right)^{1/2} \frac{k_{mn}}{\sinh(2k_{mn}H)} + \left(\frac{\omega_{mn}}{2Re}\right)^{1/2} \left[ \frac{1}{2} \frac{1 + (m/k_{mn})}{1 - (m/k_{mn})} - \frac{k_{mn}H}{\sinh(2k_{mn}H)} \right], \quad (\text{A } 1)$$

where the first term represents the bulk dissipation, whereas the second and third terms are related to the dissipation occurring at the solid bottom and sidewall, respectively. In equation (A 1),  $H = h/R$  is the non-dimensional fluid depth,  $k_{mn}$  is the non-dimensional wavenumber associated with mode  $(m, n)$ ,  $\omega_{mn}$  is the corresponding natural frequency obeying to the dispersion relation (3.6) and  $Re = g^{1/2}R^{3/2}/\nu$  is the Reynolds number ( $\nu$  denotes the kinematic viscosity of the fluid). In §4.2.2 an amplitude equation, governing the dynamics of a natural mode  $(2, n)$  (which leads the DC wave dynamics observed close to  $\Omega \approx \omega_{21}/2$ ), was derived. For mode  $(2, 1)$  in the conditions of figure 6, i.e. pure water with  $\rho = 1000\text{kg/m}^3$ ,  $\gamma = 0.072\text{N/m}$ ,  $\nu = 1 \times 10^{-6}\text{m}^2/\text{s}$ ,  $D = 0.144\text{m}$  (for which the Bond number is  $Bo = 705.6$ ) and  $H = 1.04 = 2\tilde{H}$ , the values  $Re = 60480$ ,  $k_{21} = 3.0542$  and  $\omega_{21} = 1.7561$  give a non-dimensional viscous damping coefficient  $\sigma = 0.0051$ , mostly produced by the sidewall boundary layer. Typically, as in the present case and as supported by experimental (Cocciaro *et al.* 1993) and numerical (Viola *et al.* 2018) evidences, the viscous damping rate can be interpreted as a slow damping process over a faster time scale represented by the wave oscillation. Under this hypothesis, which translates in the assumption of a viscous damping coefficient of order  $\epsilon^2$  within the present WNL framework, the damping coefficient can be added *a posteriori*, i.e. in a phenomenological way, to the final inviscid amplitude equation from (4.22), leading to

$$\frac{dB}{dt} = - [\sigma + i(2\lambda - \chi_{DC}f^2)] B + i(\zeta_{DC}\lambda + \mu_{DC})f^2 + i\nu_{DC}|B|^2B. \quad (\text{A } 2)$$

The stationary form of (A 2) can be rearranged in the following implicit form

$$(2\lambda - \nu_{DC}|B|^2 - \chi_{DC}f^2)|B| \pm \sqrt{f^4(\zeta_{DC}\lambda + \mu_{DC})^2 - (\sigma|B|)^2} = 0, \quad (\text{A } 3)$$

which can be solved using the Matlab function *fimplicit*. The effect of viscous dissipation on the DC regime is investigated in figure 9 for two representative values of the shaking diameter.

The case of figure 9(a) shows that the so-called jump-down frequency is somewhere in between  $\Omega \in [0.675, 0.685]$ . The damping value produced by (A 1) appears to be too small to match the experimental jump-down frequency, hence we tentatively added a pre factor in order to fit the measurements. It turns out that a pre factor of 1.35 is sufficient to provide a fairly good prediction of the jump-down frequency. We note that prediction (A 1) does not involve any dissipation mechanism associated with the contact



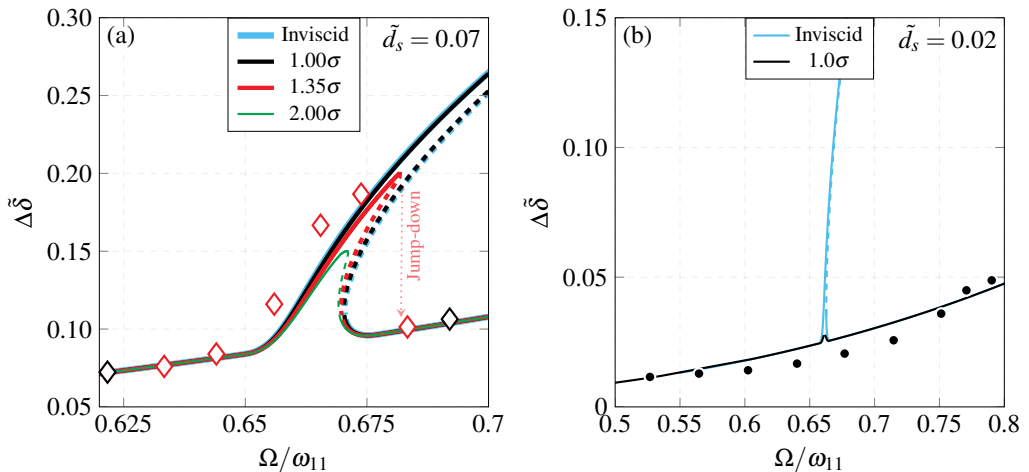


FIGURE 9. (a) Same case of figure 6-(a) with  $\tilde{d}_s = 0.07$ . (b) same as (a), but for  $\tilde{d}_s = 0.02$  (from figure 2), value at which the double-crest dynamics does not manifest. Solid and dashed lines correspond to stable and unstable branches, respectively, computed via the weakly nonlinear analysis in the inviscid case and for different values of damping coefficient, with  $\sigma$  given by (A 1). Markers correspond to the experimental points shown in figure 2 and extracted from Reclari *et al.* (2014).

line, i.e. contact line hysteresis (Miles 1967; Cocciaro *et al.* 1993; Dussan 1979; Hocking 1987; Keulegan 1959; Kidambi 2009; Viola *et al.* 2018; Viola & Gallaire 2018) or possible surface contamination (Henderson & Miles 1990, 1994). Indeed, depending on the configuration, contact line dynamics may rule the overall dissipation, with a measured damping coefficient up to 10-20 times larger (Benjamin & Ursell 1954; Hocking 1987; Kidambi 2009) than that predicted by (A 1). Comparison of the theoretical damping coefficient value with that measured in moving contact line experiments, due to unavoidable sources of uncertainty in the meniscus dynamics, have always been mostly qualitative, rather than quantitative, requiring often the use of fitting parameters. For instance, in their predictive theory for single-mode Faraday experiments, Henderson & Miles (1990) used an effective fluid viscosity 3 times larger than the actual one. Recently, Bäuerlein & Avila (2021) have measured the damping coefficient of the first anti-symmetric sloshing mode in a quasi-two-dimensional rectangular container, which was seen to be approximately 1.5 larger than that predicted by the theory (Faltinsen & Timokha 2009). The need for a pre factor of 1.35 in figure 9(a), which approximately corresponds to a fictitious fluid with a dynamic viscosity 1.8 time larger, is therefore not surprising when the damping is computed via (A 1) and contact line dissipation is neglected.

We remark that the reasonings outlined in this Appendix in order to elucidate the effect of viscosity are in fact only qualitative. Many aspects are ignored in the present inviscid analysis with phenomenological damping, two of which are commented in the following.

Prediction (A 1) is only valid for free capillary-gravity waves, whereas dissipation rates of forced wave motions are generally more complex. A proper viscous WNL analysis would produce complex eigenmodes and responses (due to the phase shift owing to viscosity) and hence complex-valued normal form coefficients. For instance, among these coefficients, the imaginary part of  $\nu_{DC}$  (or  $\nu_{SC}$ ) multiplied by  $|B|^2$  in (A 2), could be interpreted as a sort of nonlinear damping (Douady 1990),  $(\sigma + \text{Im}[\nu]|B|^2)$ ,

whose contribution to the overall dissipation mechanisms is expected to increase at larger wave amplitudes, hence influencing the location of the jump-down frequency. In contradistinction with the case of a pinned (or fixed) contact line, a formal viscous analysis undertaking the case of a moving contact line would require the introduction of a slip length model in order to regularize the well-known contact line stress-singularity (Huh & Scriven 1971; Davis 1974; Lauga *et al.* 2007; Navier 1823; Viola & Gallaire 2018).

Most importantly, the inviscid WNL model is not capable to describe the continuous modulation of the phase lag between the external forcing and the wave amplitude response, which has been recently demonstrated by Bäuerlein & Avila (2021) (for uni-directional sloshing waves in three-dimensional rectangular container) to be of crucial importance in the correct prediction of the jump-down frequency, otherwise often inaccurate, even when the considered damping coefficient is that measured experimentally. In principle, a formal viscous analysis, as briefly introduced above, is expected to correctly capture such a phase lag.

Another interesting case, that is worth to be commented, is that shown in figure 9(b). At a shaking diameter  $\tilde{d}_s = 0.02$  (the lowest reported in figure 2), the DC dynamics was not observed at all. This is in conflict with the inviscid straightforward asymptotic analysis, which always prescribes a divergent behaviour close to the dominant super-harmonic,  $\Omega \approx \omega_{21}/2$ , even for vanishing  $\tilde{d}_s$ . However, as soon as viscous dissipation is introduced, the energy pumped into the system is not sufficient to overcome dissipative effects and DC waves are essentially suppressed, with a system responses that follows satisfactorily the linear solution (see figure 2) showing a single-crest dynamics ranging over the whole frequency window,  $\Omega/\omega_{11} \in [0, 1]$ , in agreement with experimental evidences.

## Appendix B. Asymptotic harmonic solution of the undamped Duffing equation

By analogy with the weakly nonlinear analysis for harmonic single-crest wave dynamics presented in §4.1, we look for an asymptotic solution of the undamped Duffing equation

$$\ddot{x} + x + c_3 x^3 = p \cos \Omega t, \quad (\text{B1})$$

having the form  $x = x_0 + \epsilon x_1$ . Additionally, as standard in asymptotic solutions of the Duffing equation, we assume a small external forcing amplitude,  $p = \epsilon \hat{p}$  and detuning from the exact resonance, i.e.  $\Omega = 1 + \lambda = 1 + \epsilon \hat{\lambda}$ , small nonlinearities through  $c_3 = \epsilon \hat{c}_3$  and the existence of a characteristic slow time scale  $\hat{t}_1 = \epsilon t$ . Under these assumptions, the  $\epsilon^0$ -order homogeneous solutions simply reads

$$x_0 = C(\hat{t}_1) e^{it} + c.c.. \quad (\text{B2})$$

with  $C(\hat{t}_1)$  to be determined at next order. At order  $\epsilon$  one can readily verify that, in order to avoid secular terms, a solvability condition must be satisfied. Such a condition leads to the very classical amplitude equation

$$dD/dt = -i\lambda D + i(-1/4)p + i(3c_3/2)|D|^2 D, \quad (\text{B3})$$

where the change of variable  $C = D e^{i\lambda t}$  was introduced and each quantity was recast in terms of the corresponding physical value (to eliminate the implicit small parameter  $\epsilon$ ).

By noticing that

$$-1/4 \leftrightarrow \mu_{SC}, \quad 3c_3/2 \leftrightarrow \nu_{SC}, \quad (\text{B } 4)$$

one immediately recognizes that equation (4.6) has indeed the same structure of the formal amplitude equation (B 3), thus suggesting that the continuous sloshing system and the one-degree-of-freedom (1dof) Duffing system, under the specific conditions listed above, behave essentially in the same way.

### Appendix C. Asymptotic super-harmonic solution of the undamped Helmholtz–Duffing equation

In this Appendix, although with the additional assumption of vanishing damping, we briefly summarize the super-harmonic weakly nonlinear solution of the Helmholtz–Duffing equation,

$$\ddot{x} + x + c_2x^2 + c_3x^3 = p \cos \Omega t, \quad (\text{C } 1)$$

derived by Benedettini & Rega (1989) and introduced in §4.1.

We look for an asymptotic solution of the form  $x = x_0 + \epsilon x_1 + \epsilon^2 x_2$ , to equation (C 1) with  $\sigma = 0$  (undamped oscillator),  $2\Omega = 1 + \lambda = 1 + \epsilon \hat{\lambda}$  and with small nonlinearities through  $c_2 = \epsilon \hat{c}_2$  and  $c_3 = \epsilon^2 \hat{c}_3$  (with the cubic term one order smaller than the quadratic one). The existence of a two slow time scales is hypothesized,  $\hat{t}_1 = \epsilon t$  and  $\hat{t}_2 = \epsilon^2 t$ . Under these assumptions, the solution of the  $\epsilon^0$ -order forced linear problem reads

$$x_1 = C(\hat{t}_1, \hat{t}_2) e^{it} + f e^{i(1/2)t} e^{i(\lambda/2)\hat{t}_1} + c.c., \quad (\text{C } 2)$$

with  $f = (2/3)p$  and  $C(\hat{t}_1, \hat{t}_2)$  to be determined at next order. At orders  $\epsilon$  and  $\epsilon^2$ , resonating terms produced by the weak quadratic and cubic nonlinearities, respectively, arise, thus requiring the imposition of two solvability conditions prescribing that amplitude  $C(\hat{t})$  must obey to the following normal forms

$$\boxed{\epsilon^1} : \quad dC/d\hat{t}_1 = i(c_2/2) f^2 e^{i\lambda \hat{t}_1}, \quad (\text{C } 3a)$$

$$\boxed{\epsilon^2} : \quad dC/d\hat{t}_2 = -i\hat{\lambda}(c_2/4) e^{i\lambda \hat{t}_1} - i c_5 f^2 A - i 4c_4 |C|^2 C, \quad (\text{C } 3b)$$

with the full expression of the auxiliary coefficients  $c_4$  and  $c_5$  (both functions of  $c_2$  and  $c_3$ ), given in Benedettini & Rega (1989). Combining (C 3a) and (C 3b) into a single amplitude equation (by summing the two expression by their respective weights, i.e.  $\epsilon$  and  $\epsilon^2$ , and reintroducing the physical quantities in order to eliminate the dependence on the implicit small parameter  $\epsilon$ ), one obtains

$$dD/dt = -i(\lambda + c_5 f^2) D + i(1 - \lambda/2) c_2 f^2 / 2 - i 4c_4 |D|^2 D, \quad (\text{C } 4)$$

with  $C = D e^{i\lambda t}$ . Note that the procedure used in the perturbation analysis above and outlined in Benedettini & Rega (1989) is in fact equivalent to that followed in Nayfeh (1984) for treating the same second order super-harmonic resonance in a more general case of a two-term excitation. By comparing the various terms of (C 4) with those of (4.22), the analogy is evident, thus suggesting that the actual inviscid sloshing dynamics in the double-crest wave regime may be, at least qualitatively, described by the undamped Helmholtz–Duffing equation (4.26) driven super-harmonically.

## Acknowledgements

We acknowledge Mohamed Farhat for fruitful discussions.

## Funding

We acknowledge the Swiss National Science Foundation under grant 200021\_178971.

## Declaration of Interests

The authors report no conflict of interest.

## REFERENCES

- ALIJANI, F., BAKHTIARI-NEJAD, F. & AMABILI, M. 2011 Nonlinear vibrations of fgm rectangular plates in thermal environments. *Nonlinear Dyn.* **66** (3), 251–270.
- ASKARI, H., SAADATNIA, Z., YOUNESIAN, D., YILDIRIM, A. & KALAMI-YAZDI, M. 2011 Approximate periodic solutions for the Helmholtz–Duffing equation. *Comput. Math. Appl.* **62** (10), 3894–3901.
- BAUER, H. F. 1966 Nonlinear mechanical model for the description of propellant sloshing. *AIAA* **4** (9), 1662–1668.
- BÄUERLEIN, B. & AVILA, K. 2021 Phase lag predicts nonlinear response maxima in liquid-sloshing experiments. *J. Fluid Mech.* **925**.
- BENEDETTINI, F. & REGA, G. 1989 Planar non-linear oscillations of elastic cables under superharmonic resonance conditions. *J. Sound Vib.* **132** (3), 353–366.
- BENJAMIN, T. B. & URSELL, F. J. 1954 The stability of the plane free surface of a liquid in vertical periodic motion. *Proc. R. Soc. A: Math. Phys. Eng. Sci.* **225** (1163), 505–515.
- BOUVARD, J., HERREMAN, W. & MOISY, F. 2017 Mean mass transport in an orbitally shaken cylindrical container. *Phys. Rev. Fluids* **2** (8), 084801.
- BREMER, T. S. VAN DEN & BREIVIK, Ø. 2018 Stokes drift. *Philos. Trans. Royal Soc. A PHILOS T R SOC A* **376** (2111).
- BÜCHS, J. 2001 Introduction to advantages and problems of shaken cultures. *Biochem. Eng. J.* **7** (2), 91–98.
- BÜCHS, J., MAIER, U., MILBRADT, C. & ZOELS, B. 2000a Power consumption in shaking flasks on rotary shaking machines: I. power consumption measurement in unbaffled flasks at low liquid viscosity. *Biotechnol. Bioeng.* **68** (6), 589–593.
- BÜCHS, J., MAIER, U., MILBRADT, C. & ZOELS, B. 2000b Power consumption in shaking flasks on rotary shaking machines: II. nondimensional description of specific power consumption and flow regimes in unbaffled flasks at elevated liquid viscosity. *Biotechnol. Bioeng.* **68** (6), 594–601.
- CASE, K. M. & PARKINSON, W. C. 1957 Damping of surface waves in an incompressible liquid. *J. Fluid Mech.* **2** (2), 172–184.
- CASTAING, B. 2005 *Hydrodynamics and nonlinear instabilities*, vol. 3. Cambridge University Press.
- CENEDESE, M. & HALLER, G. 2020 How do conservative backbone curves perturb into forced responses? a melnikov function analysis. *Proc. R. Soc. A: Math. Phys. Eng. Sci.* **476** (2234), 20190494.
- COCCIARO, B., FAETTI, S. & FESTA, C. 1993 Experimental investigation of capillarity effects on surface gravity waves: non-wetting boundary conditions. *J. Fluid Mech.* **246**, 43–66.
- DAVIS, S. H. 1974 On the motion of a fluid-fluid interface along a solid surface. *J. Fluid Mech.* **65** (1), 71–95.
- DODGE, F. T. 2000 *The new "Dynamic Behavior of Liquids in Moving Containers"*. Southwest Research Inst. San Antonio, TX.
- DODGE, F. T., KANA, D. D. & ABRAMSON, H. N. 1965 Liquid surface oscillations in longitudinally excited rigid cylindrical containers. *AIAA* **3** (4), 685–695.
- DOUADY, S. 1990 Experimental study of the Faraday instability. *J. Fluid Mech.* **221**, 383–409.
- DUFFING, G. 1918 *Erzwungene Schwingungen bei veränderlicher Eigenfrequenz und ihre technische Bedeutung*. Vieweg.

- DUSSAN, E. B. 1979 On the spreading of liquids on solid surfaces: static and dynamic contact lines. *Annu. Rev. Fluid Mech.* **11** (1), 371–400.
- FALLAH, A. & AGHDAM, M. M. 2011 Nonlinear free vibration and post-buckling analysis of functionally graded beams on nonlinear elastic foundation. *Eur. J. Mech. A. Solids* **30** (4), 571–583.
- FALTINSEN, O. M. 1974 A nonlinear theory of sloshing in rectangular tanks. *J. Sh. Res.* **18** (04), 224–241.
- FALTINSEN, O. M., LUKOVSKY, I. A. & TIMOKHA, A. N. 2016 Resonant sloshing in an upright annular tank. *J. Fluid Mech.* **804**, 608–645.
- FALTINSEN, O. M., ROGNEBAKKE, O. F. & TIMOKHA, A. N. 2005 Resonant three-dimensional nonlinear sloshing in a square-base basin. part 2. effect of higher modes. *J. Fluid Mech.* **523**, 199–218.
- FALTINSEN, O. M. & TIMOKHA, A. N. 2009 *Sloshing*. Cambridge University Press.
- FRIEDRICHS, K. O. 2012 *Spectral theory of operators in Hilbert space*. Springer Science & Business Media.
- HANDA-CORRIGAN, A., EMERY, A. N. & SPIER, R. E. 1989 Effect of gas–liquid interfaces on the growth of suspended mammalian cells: mechanisms of cell damage by bubbles. *Enzyme Microb. Technol.* **11** (4), 230–235.
- HENDERSON, D. M. & MILES, J. W. 1990 Single-mode faraday waves in small cylinders. *J. Fluid Mech.* **213**, 95–109.
- HENDERSON, D. M. & MILES, J. W. 1994 Surface-wave damping in a circular cylinder with a fixed contact line. *J. Fluid Mech.* **275**, 285–299.
- HOCKING, L. M. 1987 The damping of capillary–gravity waves at a rigid boundary. *J. Fluid Mech.* **179**, 253–266.
- HORSTMANN, G. M., ANDERS, S., KELLEY, D. H. & WEIER, T. 2021 Formation of spiral waves in cylindrical containers under orbital excitation. *J. Fluid Mech.* **925**.
- HORSTMANN, G. M., HERREMAN, W. & WEIER, T. 2020 Linear damped interfacial wave theory for an orbitally shaken upright circular cylinder. *J. Fluid Mech.* **891**.
- HUH, C. & SCRIVEN, L. E. 1971 Hydrodynamic model of steady movement of a solid/liquid/fluid contact line. *J. Colloid Interface Sci.* **35** (1), 85–101.
- IBRAHIM, R. A. 2005 *Liquid sloshing dynamics: theory and applications*. Cambridge University Press.
- JESUS, M. J. DE, GIRARD, P., BOURGEOIS, M., BAUMGARTNER, G., JACKO, B., AMSTUTZ, H. & WURM, F. M. 2004 Tubespinn satellites: a fast track approach for process development with animal cells using shaking technology. *Biochem. Eng. J.* **17** (3), 217–223.
- JORDAN, D. W. & SMITH, P. 1999 *Nonlinear ordinary differential equations: an introduction to dynamical systems*, vol. 2. Oxford University Press, USA.
- KALMÁR-NAGY, T. & BALACHANDRAN, B. 2011 Forced harmonic vibration of a Duffing oscillator with linear viscous damping. *The duffing equation: nonlinear oscillators and their behaviour* pp. 139–174.
- KE, L.-L., YANG, J. & KITIPORNCHAI, S. 2010 An analytical study on the nonlinear vibration of functionally graded beams. *Meccanica* **45** (6), 743–752.
- KEULEGAN, G. H. 1959 Energy dissipation in standing waves in rectangular basins. *J. Fluid Mech.* **6** (1), 33–50.
- KIDAMBI, R. 2009 Capillary damping of inviscid surface waves in a circular cylinder. *J. Fluid Mech.* **627**, 323–340.
- KLÖCKNER, W. & BÜCHS, J. 2012 Advances in shaking technologies. *Trends Biotechnol.* **30** (6), 307–314.
- KOVACIC, I. & BRENNAN, M. J. 2011 *The Duffing equation: nonlinear oscillators and their behaviour*. John Wiley & Sons.
- KRETZMER, G. & SCHÜGERL, K. 1991 Response of mammalian cells to shear stress. *Appl. Microbiol. Biotechnol.* **34** (5), 613–616.
- LAMB, H. 1993 *Hydrodynamics*. Cambridge university press.
- LAUGA, ERIC, BRENNER, MICHAEL & STONE, HOWARD 2007 *Microfluidics: The No-Slip Boundary Condition*, pp. 1219–1240. Berlin, Heidelberg: Springer Berlin Heidelberg.
- LIU, C.-M. & HONG, L.-N. 2001 Development of a shaking bioreactor system for animal cell cultures. *Biochem. Eng. J.* **7** (2), 121–125.

- LUKOVSKY, I. A. 1990 Introduction to nonlinear dynamics of a solid body with a cavity including a liquid. *Kiev: Naukova dumka (in Russian)* .
- MAIER, U., LOSEN, M. & BÜCHS, J. 2004 Advances in understanding and modeling the gas-liquid mass transfer in shake flasks. *Biochem. Eng. J.* **17** (3), 155–167.
- MCDANIEL, L. E. & BAILEY, E. G. 1969 Effect of shaking speed and type of closure on shake flask cultures. *Appl. Microbiol.* **17** (2), 286–290.
- MELIGA, P., GALLAIRE, F. & CHOMAZ, J. M. 2012 A weakly nonlinear mechanism for mode selection in swirling jets. *J. Fluid Mech.* **699**, 216–262.
- MICHELETTI, M., BARRETT, T., DOIG, S. D., BAGANZ, F., LEVY, M. S., WOODLEY, J. M. & LYE, G. J. 2006 Fluid mixing in shaken bioreactors: Implications for scale-up predictions from microlitre-scale microbial and mammalian cell cultures. *Chem. Eng. Sci.* **61** (9), 2939–2949.
- MILES, J. W. 1967 Surface-wave damping in closed basins. *Proc. R. Soc. A: Math. Phys. Eng. Sci.* **297**, 459–475.
- MILES, J. W. 1984a Internally resonant surface waves in a circular cylinder. *J. Fluid Mech.* **149**, 1–14.
- MILES, J. W. 1984b Resonantly forced surface waves in a circular cylinder. *J. Fluid Mech.* **149**, 15–31.
- MIRZABEIGY, A., YAZDI, M. K. & NASEHI, M. H. 2014 Approximate periodic solution for the nonlinear Helmholtz-Duffing oscillator via analytical approaches. *Int. J. Comput. Math.* **2014**.
- MOISEEV, N. N. 1958 On the theory of nonlinear vibrations of a liquid of finite volume. *J. Appl. Math. Mech.* **22** (5), 860–872.
- MOISY, F., BOUVARD, J. & HERREMAN, W. 2018 Counter-rotation in an orbitally shaken glass of beer. *EPL* **122** (3), 34002.
- MULLER, N., DEROUAZI, M., TILBORGH, F. VAN, WULHFARD, S., HACKER, D. L., JORDAN, M. & WURM, F. M. 2007 Scalable transient gene expression in chinese hamster ovary cells in instrumented and non-instrumented cultivation systems. *Biotechnol. Lett.* **29** (5), 703–711.
- MULLER, N., GIRARD, P., HACKER, D. L., JORDAN, M. & WURM, F. M. 2005 Orbital shaker technology for the cultivation of mammalian cells in suspension. *Biotechnol. Bioeng.* **89** (4), 400–406.
- NARIMANOV, G. S. 1957 Movement of a tank partly filled by a fluid: the taking into account of non-smallness of amplitude. *Prikl. Math. Mech. (in Russian)* **21**, 513–524.
- NARIMANOV, G. S., DOKUCHAEV, L. V. & LUKOVSKY, I. A. 1977 Nonlinear dynamics of flying apparatus with liquid. moscow: Mashinostroenie. (*in Russian*) .
- NAVIER, C. L. M. H. 1823 Mémoire sur les lois du mouvement des fluides. *Mém. Acad. R. des Sci. Inst. France* **6** (1823), 389–440.
- NAYFEH, A. H. 1984 Quenching of primary resonance by a superharmonic resonance. *J. Sound Vib.* **92** (3), 363–377.
- NAYFEH, A. H. 2008 *Perturbation Methods*. Wiley.
- OCKENDON, J. R. & OCKENDON, H. 1973 Resonant surface waves. *J. Fluid Mech.* **59** (2), 397–413.
- ORCHINI, A., RIGAS, G. & JUNIPER, M. P. 2016 Weakly nonlinear analysis of thermoacoustic bifurcations in the rijke tube. *J. Fluid Mech.* **805**, 523–550.
- PAPOUTSAKIS, E. T. 1991 Fluid-mechanical damage of animal cells in bioreactors. *Trends Biotechnol.* **9** (1), 427–437.
- RAYNOVSKYY, I. & TIMOKHA, A. N. 2018 Steady-state resonant sloshing in an upright cylindrical container performing a circular orbital motion. *Math. Probl. Eng.* .
- RECLARI, M. 2013 Hydrodynamics of orbital shaken bioreactors. *Tech. Rep.*. EPFL.
- RECLARI, M., DREYER, M., TISSOT, S., OBRESCHKOW, D., WURM, F. M. & FARHAT, M. 2014 Surface wave dynamics in orbital shaken cylindrical containers. *Phys. Fluids* **26** (5), 052104.
- REGA, G. 1995 Bifurcation and chaos in the Helmholtz-Duffing oscillator. In *Bifurc. Chaos*, pp. 191–215. Springer.
- TAN, R.-K., EBERHARD, W. & BÜCHS, J. 2011 Measurement and characterization of mixing time in shake flasks. *Chem. Eng. Sci.* **66** (3), 440–447.

- TIMOKHA, A. N. & RAYNOVSKYY, I. 2017 The damped sloshing in an upright circular tank due to an orbital forcing. *Dopov. Nats. Akad. Nauk. Ukr.* **10**, 48–53.
- TISSOT, S., FARHAT, M., HACKER, D. L., ANDERLEI, T., KÜHNER, M., COMNINELLIS, C. & WURM, F. M. 2010 Determination of a scale-up factor from mixing time studies in orbitally shaken bioreactors. *Biochem. Eng. J.* **52** (2-3), 181–186.
- TISSOT, S., OBERBEK, A., RECLARI, M., DREYER, M., HACKER, D. L., BALDI, L., FARHAT, M. & WURM, F. M. 2011 Efficient and reproducible mammalian cell bioprocesses without probes and controllers? *New Biotechnol.* **28** (4), 382–390.
- VIOLA, F., BRUN, P.-T. & GALLAIRE, F. 2018 Capillary hysteresis in sloshing dynamics: a weakly nonlinear analysis. *J. Fluid Mech.* **837**, 788–818.
- VIOLA, F. & GALLAIRE, F. 2018 Theoretical framework to analyze the combined effect of surface tension and viscosity on the damping rate of sloshing waves. *Phys. Rev. Fluids* **3** (9), 094801.
- WURM, F. M. 2004 Production of recombinant protein therapeutics in cultivated mammalian cells. *Nat. Biotechnol.* **22** (11), 1393–1398.
- ZHANG, X., BÜRKI, C., STETTLER, M., SANCTIS, D. DE, PERRONE, M., DISCACCIATI, M., PAROLINI, N., DEJESUS, M., HACKER, D. L., QUARTERONI, A. & WURM, F. M. 2009 Efficient oxygen transfer by surface aeration in shaken cylindrical containers for mammalian cell cultivation at volumetric scales up to 1000 l. *Biochem. Eng. J.* **45** (1), 41–47.